Evidence for upward but not downward influence between the wintertime troposphere and stratosphere

Kara Hartig,[a] Nili Harnik,[b] and Eli Tziperman,[c,d]

[a] *Department of Physics, Harvard University, Cambridge, Massachusetts*

[b] *Department of Geosciences, Tel Aviv University, Tel Aviv, Israel*

[c] *Department of Earth & Planetary Sciences, Harvard University, Cambridge, Massachusetts*

[d] *School of Engineering and Applied Sciences, Harvard University, Cambridge, Massachusetts*

Corresponding author: Kara Hartig, kara_hartig@g.harvard.edu

ABSTRACT: The past few decades of work on stratosphere-troposphere teleconnections have been unable to reach a consensus on either the time scale or consequences for weather of upward and downward propagation. In an attempt to identify significant patterns of covariance between the surface and stratosphere without imposing an expected pattern or timescale, we apply Maximum Covariance Analysis (MCA) with a variable time lag between pairs of tropospheric and stratospheric fields. Using over 60 years of ERA5 reanalysis for Northern Hemisphere winters, we use MCA to pick out the time lags and patterns corresponding to the largest covariance between the surface and the stratosphere. We find that the greatest covariance occurs when the surface precedes the stratosphere by up to 9 days, corresponding to a sea level pressure anomaly with one pole over Alaska and another north of the Caspian Sea that is followed by changes in stratospheric potential vorticity, zonal wind, and EP flux. A second sea level pressure anomaly, similar to the first but rotated about the pole by about 60°, was also found to precede stratospheric EP flux variations 2–3 days later, although this pattern does not appear as closely related to potential vorticity and zonal wind in the stratosphere. We find little evidence for a downward influence beyond about 3 days, and the influence we do find affects sea level pressure but not minimum surface temperatures.

SIGNIFICANCE STATEMENT: We seek to improve both predictability and fundamental understanding of the linkages between the troposphere, the convectively active layer of the atmosphere responsible for weather, and the stratosphere, the much more stable region just above it. We identify two timescales of upward influence from the surface to the stratosphere, one of two to three days and the other around nine days, with distinct precursors at the surface. While we also find a downward influence of the stratosphere on the Northern Annular Mode, the corresponding time scale of three days is shorter than previous work has suggested, and this influence does not extend to a noticeable impact on surface temperatures.

1. Introduction

Compared to the troposphere, which is agitated by convection, surface forcings, and dynamic variability on all spatial scales, the stratosphere has fewer sources of variability. Dynamic variability in the extratropical stratosphere is strongly dominated on the seasonal scale by the formation and breakdown of the stratospheric polar vortex, which forms in the winter hemisphere, and on the sub-seasonal scale by upward propagation of planetary waves that occasionally result in dramatic disruptions of that vortex during Sudden Stratospheric Warmings (SSWs; Andrews et al. 1987; Polvani and Waugh 2004; Butler et al. 2015; Baldwin et al. 2021). While the upward influence of the troposphere on the stratosphere is well-established, it has also been suggested that the stratosphere, even with its much lower mass, is, in turn, capable of substantially influencing surface weather through a downward influence. But in spite of significant effort, the characteristics and mechanisms of a downward influence are still not completely understood. Our aim is to identify the time scales and spatial patterns that characterize teleconnections, both upward and downward, between stratospheric and tropospheric fields using Maximum Covariance Analysis applied to reanalysis data.

SSWs are the most dramatic evidence of the *upward* influence of the surface on the stratosphere. In winter, planetary waves of low wavenumber excited in the troposphere can propagate upward into the polar stratosphere (Charney and Drazin 1961). When these waves break and deposit momentum in a wave-mean flow interaction (Matsuno 1971; McIntyre and Palmer 1984; Plumb 2010), they decelerate the polar jet, resulting in a positive feedback that allows more waves to propagate upward and subsequently break, further decelerating the jet. This wave-breaking feedback can lead

to an SSW: a displacement, split, or collapse of the polar vortex that can increase stratospheric temperatures over the pole by 40 °C or more in a matter of days (Andrews et al. 1987; Butler et al. 2015; Kidston et al. 2015; Labitzke and Kunze 2009). SSWs occur roughly six times per decade in the Northern Hemisphere (Butler et al. 2015) but have an outsized impact on the stratosphere, as the resultant temperature and wind anomalies can take over a month to return to the background state (Limpasuvan et al. 2004). Surface precursors to SSWs have been identified that are consistent with the mechanism of upward propagation of wavenumbers 1 and 2, including blocking (Quiroz 1986; Andrews et al. 1987; Martius et al. 2009) and sea level pressure or geopotential height anomalies (Ambaum and Hoskins 2002; Garfinkel et al. 2010; Kolstad et al. 2010; Lehtonen and Karpechko 2016; Domeisen et al. 2020). But the presence of these precursors does not consistently lead to SSWs (Martius et al. 2009), motivating recent work emphasizing the importance of the stratospheric state in addition to tropospheric wave activity in generating SSWs (Birner and Albers 2017).

A *downward* influence from the polar stratosphere on tropospheric weather is not as well-established. The strongest line of evidence for a downward influence appears in changes to the northern annular mode (NAM), which explains a large fraction of the variance in the extratropical circulation and is defined by the first empirical orthogonal function of wintertime geopotential height at a given pressure (Baldwin 2001; Thompson and Wallace 2001). Baldwin and Dunkerton (2001) used composites of 90-day low-pass filtered NAM anomalies following SSWs to identify what appeared to be a downward propagation of the negative NAM phase from the stratosphere to the surface over the course of two to three weeks, a result which subsequent studies have successfully replicated (Mitchell et al. 2013; Sigmond et al. 2013; Hitchcock and Simpson 2014), although Hitchcock and Simpson (2014) point out that the signal in the troposphere is marginal at the 95% level. The two phases of the NAM correspond to significant differences in storminess and cold air outbreaks (Marshall et al. 2001; Thompson and Wallace 2001; Hurrell et al. 2003), implying that SSWs could influence surface weather by propagating a negative NAM phase to the surface (Scaife et al. 2005; Kidston et al. 2015; Lee et al. 2019). But a direct link between stratospheric variability and surface weather impacts has not been established beyond a few specific cases (Albers et al. 2022; Zhang et al. 2022), obstructing efforts to use stratospheric variability to extend the lead time on weather forecasts.

At least three mechanisms by which the stratosphere might exert a downward influence on the surface have been suggested. The first involves a wave-mean flow interaction. As upward propagating waves break in the stratosphere, they decelerate the zonal wind and move the critical layer down, forcing the next wave to break lower. In this fashion, a series of waves causes the deceleration of the zonal wind to migrate down through the stratosphere until it reaches the tropopause and begins to modulate tropospheric wave activity (Holton and Mass 1976; Kodera et al. 2000; Limpasuvan et al. 2004). Downward migration of zonal-mean zonal wind anomalies has been observed in reanalysis (Baldwin and Dunkerton 1999; Kuroda and Kodera 1999) and models (Christiansen 2001; Plumb and Semeniuk 2003) and linked to a negative annular mode phase at the surface (Baldwin and Dunkerton 2001; Thompson et al. 2002; Limpasuvan et al. 2004; Thompson et al. 2005), consistent with this mechanism. The second mechanism acts through wave reflection. Negative vertical zonal wind shear in the upper stratosphere can form a reflecting surface, causing upward propagating waves to reflect back down into the troposphere instead of being absorbed through the wave-mean flow interaction (Randel 1987; Harnik and Lindzen 2001; Perlwitz and Harnik 2003, 2004; Harnik 2009; Shaw et al. 2010). Kodera et al. (2016) found that SSWs that result in wave reflection, identified by a downward EP flux at 100 hPa, tend to amplify the stationary wave pattern in the mid-troposphere, thus creating a downward influence on tropospheric activity and possibly surface weather. The third mechanism involves a redistribution of mass over the polar cap. Observations have found that mass moves into the polar cap following an SSW, raising Arctic surface pressure and projecting onto the negative phase of the NAM (Baldwin and Dunkerton 2001; Mitchell et al. 2013; Sigmond et al. 2013; Hitchcock and Simpson 2014). The mechanisms for this redistribution have not been fully explained, but appear to include synoptic-scale eddy feedbacks and a stratospheric influence on planetary-scale momentum flux (Simpson et al. 2009; Domeisen et al. 2013; Hitchcock and Simpson 2016). Our analysis here will remain largely agnostic regarding which mechanism is more robust or occurs more frequently. Instead, we are looking for statistical evidence of such a downward influence over a wide range of time scales and multiple fields, evidence that one expects regardless of which mechanism is involved.

Progressing from the impact of SSWs on the NAM to an impact on surface weather extremes has introduced additional uncertainty. The best agreement across studies identifies a warm surface air temperature anomaly over the Labrador Sea and cooling over northern Russia on the order of

1–3 K one to two months after an SSW (Thompson et al. 2002; Kolstad et al. 2010; Lehtonen and Karpechko 2016; Ayarzagüena et al. 2020). However, there is little consensus on the temperature response over populated mid-latitude coastal areas, and even less that holds across multiple data sets or models and is statistically significant. Taking North America (away from the Labrador Sea) as an example, studies have found an overall cold anomaly (Thompson et al. 2002), an increase in the number of cold days (Zhang et al. 2020; Thompson et al. 2002), or an increase in the area experiencing anomalously cold temperatures (Yu et al. 2018) following SSWs. However, others have found no significant signal over North America or disagreement across models and with reanalysis (Lehtonen and Karpechko 2016; Ayarzagüena et al. 2020). The implications for surface weather are further complicated by the possibility of multiple sub-types of SSWs with distinct surface responses which are washed out in the average. For example, Mitchell et al. (2013) found that displacement SSWs, in which the vortex is shifted off the pole, have a distinct surface temperature response from split SSWs, in which the vortex divides into two smaller vortices, but others have found little difference when separating by event type (Lehtonen and Karpechko 2016; Charlton and Polvani 2007; White et al. 2020). By contrast, Kodera et al. (2016) argued that the tropospheric response should be more closely related to the vertical structure of planetary waves than to the horizontal geometry of the vortex. Distinguishing between absorbing and reflecting SSWs, they found a NAM-like response at the surface following absorbing events but an amplification of the stationary planetary wave structure following reflecting events. The sensitivity to the design of each study could indicate that the surface signal is too weak or varies widely from one SSW to another, in which case it may be of little interest for extreme weather prediction. But it could also mean that the time window or SSW sub-type classifications used so far are not a good representation of the relevant dynamics, in which case an analysis method that does not presuppose either a specific time lag or stratospheric dynamical feature is desirable, such as the one we will pursue below.

Looking ahead towards the end of the 21st century, there remains much uncertainty regarding the role that climate change will have in both upward and downward propagation. Some GCMs predict more frequent SSWs in the future (Kim et al. 2017; Schimanke et al. 2013; Bell et al. 2010; Charlton-Perez et al. 2008), but these results are not conclusive and often vary across models (Butchart et al. 2000; McLandress and Shepherd 2009; Mitchell et al. 2012; Ayarzagüena et al.

2018, 2020; Rao and Garfinkel 2021), which could be the result of competing feedbacks. There is already a large natural variability among different SSWs, making it more difficult to identify a robust trend. It has been suggested, for example, that the expected strengthening of the Madden-Julien Oscillation would lead to forced planetary waves that may result in more frequent SSWs (Kang and Tziperman 2017). Changes to sea ice and snow cover consistent with global warming have been associated with an observed increase in stratospheric polar vortex stretching events (Cohen et al. 2021), which are distinct from SSWs but have also been linked to cold spells over North America (Kretschmer et al. 2018a), as well as an increased likelihood that SSWs will result in cold anomalies over Canada and the midwestern US (Zhang et al. 2020). But a recent study of 12 CMIP6 models under a $4\times CO_2$ experiment found no significant changes in the response of sea level pressure to SSWs under warming in most models (Ayarzagüena et al. 2020). In a much warmer climate, the North Atlantic Oscillation (NAO) signal may become decoupled from the Arctic Oscillation (equivalent to NAM) altogether; Hamouda et al. (2021) found that one potential consequence of this could be that the negative NAM index following SSWs no longer propagates below the tropopause by the year 2300 under a high-emission scenario. To predict how upward and downward teleconnections will change in a warming climate, it is therefore important to identify the underlying modes of covariability of the troposphere and stratosphere.

A variety of statistical analysis methods have been employed in the search for a robust signal of downward propagation from stratospheric vortex disruptions to surface weather. Composites over many SSWs of the NAM index (Baldwin and Dunkerton 2001; Mitchell et al. 2013; Hitchcock and Simpson 2014; White et al. 2020) or surface temperature anomalies (Thompson et al. 2002; Kolstad et al. 2010; Lehtonen and Karpechko 2016; Ayarzagüena et al. 2020) are widely used. But the NAM is a hemisphere-scale feature that does not necessarily translate to consistent weather extremes in any particular region, as demonstrated above. Composites over SSWs also rely on sub-type classifications that vary across studies (Butler et al. 2015), which can lead to conflicting conclusions about the existence or pattern of a surface weather response (Mitchell et al. 2013; Lehtonen and Karpechko 2016). Clustering can identify dominant patterns within the stratosphere (Kretschmer et al. 2018b,a), but links to a surface response in clustering analysis rely on compositing rather than a direct analysis of the covariance between surface and stratosphere. Additionally, while a time lag may be applied between the stratospheric cluster and the surface, there is no obvious

way to identify the optimal time lag that maximizes the covariance between the stratospheric and tropospheric fields. Maximum Covariance Analysis, which is employed in this study, (and canonical correlation analysis, a close relative) has even been used to study upward and downward propagation before (Perlwitz and Graf 1995; Christiansen 2000; Perlwitz and Harnik 2003, 2004). But those studies either did not consider a time lag or focused exclusively on wave-1 and wave-2 or zonal-mean patterns in the geopotential height, ultimately confirming that a negative NAM signal appears to lag stratospheric activity but not tying it to surface weather consequences.

We attempt to identify teleconnections between a variety of stratospheric and tropospheric fields in winter using Maximum Covariance Analysis (MCA, Bretherton et al. 1992; Perlwitz and Harnik 2003, 2004). MCA allows us to identify rather than impose the time scales and spatial patterns most relevant to the covariance between tropospheric and stratospheric fields. Using time-lagged MCA we find evidence consistent with the upward stratosphere-troposphere teleconnection, with maximal covariance when the surface precedes the 10 hPa level by about one week. However, we are unable to find much evidence of a downward influence on surface temperatures.

2. Data & Methods

Data. We use the ERA5 reanalysis product from 1959 to 2020 to investigate the covariance between stratospheric and tropospheric fields during the Northern Hemisphere winter. We analyze the 500 hPa geopotential height (Z500), sea level pressure (SLP), and the daily minimum surface air temperature (T_{min}) as representations of the tropospheric state. We also analyze the following on multiple pressure levels: Ertel potential vorticity (PV), zonal wind (U), and the negative of the vertical component of the Eliassen-Palm flux (EP) in pressure coordinates (Edmon et al. 1980), which is calculated as follows,

$$EP = -\frac{1}{d\bar{\theta}/dp} f a \cos\phi \, \overline{v'\theta'}, \tag{1}$$

where the overbar denotes a zonal average, f is the Coriolis parameter, a is the radius of the Earth, ϕ is latitude, $d\bar{\theta}/dp$ is the vertical derivative in pressure of the zonally-averaged potential temperature $\bar{\theta}$ calculated from daily output, and $\overline{v'\theta'}$ is the zonal average of the meridional wind anomaly $v' = v - \overline{v}$ multiplied by the potential temperature anomaly $\theta' = \theta - \overline{\theta}$. The negative sign counteracts the use of pressure in the vertical derivative of $\overline{\theta}$ so that positive EP corresponds to

upward flux and negative to downward. The variables v and θ are input at 6-hourly resolution into (1), after which EP is averaged over each day to produce daily means. All other fields are daily means calculated from hourly output except for surface temperature (daily minimums from hourly output). All fields are retrieved at $1^\circ \times 1^\circ$ resolution from 40°N to 90°N.

We process the data before calculating the covariance as follows. To account for the grid cell area represented by each grid point, we multiply each data field by the square root of the cosine of latitude (North et al. 1982). At each point, we remove the linear trend and the mean over the entire time span from Jan 1959 through Dec 2020. We then calculate the seasonal cycle as the day-of-year mean at each grid point, smooth the day-of-year means with a 7-day Savitzky-Golay filter of polynomial order 1 (Savitzky and Golay 1964), and subtract this smoothed seasonal cycle to convert each data field into an anomaly field. At this point, all months are included from January through December; the restriction to winter occurs in the next step in the process of introducing the time lag.

Time lag. We introduce a time lag between the tropospheric and stratospheric fields before calculating the covariance and repeat the analysis for different lags. The analysis centers on December–February, so at a time lag of zero both the tropospheric and stratospheric anomaly fields are composed of DJF for each year in the reanalysis. To introduce a time lag of n days (positive n when troposphere lags stratosphere, negative n for troposphere leads stratosphere, for $|n|$ up to 5 weeks), we consider for each year the stratospheric field from $n/2$ days *before* Dec 1 through $n/2$ days before Feb 28, and conversely the tropospheric field from $n/2$ days *after* Dec 1 through $n/2$ days after Feb 28. In this way, a timeseries at any given point in the stratosphere is always n days before (or after, for negative n) a corresponding timeseries at any given point in the troposphere. This method maximizes the amount of time spent in DJF across both fields and allows for a variable time lag of any length and either direction in time.

Time-lagged covariance. To identify the relevant teleconnection time scales, we calculate the total squared covariance as a function of the time lag between a stratospheric field and a tropospheric field (Perlwitz and Harnik 2003, 2004). We start with a stratospheric anomaly field $X = X_{(M\times N)}$, a matrix representing M grid points and N daily values, and a tropospheric field $Y = Y_{(L\times N)}$, a matrix representing L grid points and N daily values, where each column corresponds to the spatial field on a particular day written as a vector. The time-mean (average over each row) has been removed

from both X and Y. The cross-covariance matrix $C = C_{(M\times L)}$ is then,

$$C = \frac{XY^T}{N}. \tag{2}$$

Each element of C, c_{ij}, is then the lagged covariance (because X and Y are functions of the time lag) over the entire timeseries between location i in X and location j in Y. The total squared covariance (often simply "total covariance" in the text that follows) between the two fields is $\sum_{i,j} c_{ij}^2$ and is evaluated for different time lags to determine the lag that maximizes the covariance between the two fields. Note that while X and Y must have the same length along the time dimension N, they need not share a spatial dimension. For example, we can calculate C when X represents the EP flux, which is solely a function of latitude, and Y is sea level pressure, which is a function of both latitude and longitude.

Normalization. In order to display the total covariance between multiple pairs of fields on the same plot, it is helpful to define a normalized measure of the total covariance that makes sure the analysis results do not depend on the number of grid points nor on the variance of the fields involved. We chose the following normalized total covariance,

$$TSC_{norm} = \frac{ML}{min(M,L)} \frac{\sum_{i,j} c_{ij}^2}{\sum_{i,n} x_{in}^2 \sum_{j,n} y_{jn}^2}. \tag{3}$$

For the case where elements of X and Y are drawn from uniform random distributions with a mean of zero, this normalized total covariance TSC_{norm} has an expectation value of 1 when $X = Y$ and approaches 0 when X is independent of Y.

Confidence intervals. We use bootstrapped confidence intervals to estimate the uncertainty in the total covariance. Given a time lag of zero for the sake of explanation, we treat each day in DJF across all reanalysis years as a sample and randomly re-draw with replacement up to the same number of days. We then calculate the covariance matrix and total squared covariance as described above. Repeating this process 1,000 times gives us a distribution of estimates for the total covariance, from which the 90% confidence interval is determined as the range between the 5^{th} and 95^{th} percentile of the distribution of estimators. For a non-zero lag, the samples are drawn from the lagged date range for each field described above instead of just DJF. Due to the computational

intensity of this method, confidence intervals are calculated at lags of ±3 weeks and at the peak of total covariance for each pair of fields; the confidence intervals are shown as thick vertical bars in the figures that follow.

Maximum Covariance Analysis. To identify the patterns in the stratosphere and the surface that best explain the covariance between the two, we apply Maximum Covariance Analysis (MCA). MCA identifies a series of pairs of patterns (modes) of the two fields that have the maximum covariance over the data time series (Bretherton et al. 1992). To apply MCA, we use singular value decomposition on the cross-covariance matrix C,

$$C = U\Sigma V^T. \tag{4}$$

This identifies a series of mutually orthogonal modes, each characterized by a pattern in the X field (columns of U) and a corresponding pattern in the Y field (columns of V). The column vectors $\mathbf{u}_1$ and $\mathbf{v}_1$, for example, the first column of each matrix, are the most highly correlated patterns between the two fields. Note that the mode patterns $\mathbf{u}_k$ and $\mathbf{v}_k$, where k is a specific mode, are agnostic to a mutual change of sign: a given mode implies simultaneously that $\mathbf{u}_k$ and $\mathbf{v}_k$ covary and that $-\mathbf{u}_k$ and $-\mathbf{v}_k$ covary. The mode patterns returned by MCA have a vector norm of 1, although when plotting these patterns we undo the latitude weighting by dividing by the square root of the cosine of latitude and thus this unit norm is not preserved in the figures that follow.

The fraction of the total covariance between the two fields that is explained by a given mode k can be determined using the corresponding singular value σ_k in the diagonal matrix Σ,

$$\begin{matrix}\text{Fraction of covariance} \\ \text{explained by mode } k\end{matrix} = \frac{\sigma_k^2}{\sum_k \sigma_k^2}. \tag{5}$$

The singular values and corresponding mode patterns are ordered such that the first mode explains the largest fraction of the covariance between X and Y, $\sigma_1^2/\sum_k \sigma_k^2$, and each subsequent mode explains a progressively smaller fraction.

Once we have a set of K pairs of mode patterns, we can quantify their significance to the internal variability (rather than covariability) of each of the fields X and Y as well. The calculations that follow can be performed on either field, so we will use X and its corresponding mode patterns

$\mathbf{u}_k$ (a column vector from U) as an example. By projecting the original data field X onto the kth mode pattern, we define the expansion coefficient $\mathbf{a}_k = \mathbf{u}_k^T X$, which is a timeseries (a row vector) representing the strength of mode k in field X over time. We can then compute the fraction of the *variance* in a field explained by the corresponding mode pattern as,

$$\begin{matrix}\text{Fraction of variance in } X \\ \text{explained by mode pattern } \mathbf{u}_k\end{matrix} = \frac{\sum_n \mathbf{a}_k^T \mathbf{a}_k}{\sum_{i,n} x_{in}^2}, \tag{6}$$

where x_{in} is an element of the field $X_{(M\times N)}$ taken at spatial point i and time n.

3. Results

The following analysis is divided into four sections. Section 3a uses time-lagged MCA to search for time scales and patterns of covariance between the vertical EP flux and the sea level pressure. Section 3b expands this analysis to all pairs of tropospheric and stratospheric fields under consideration to identify and interpret shared time scales and covarying modes of upward influence. Section 3c follows up with the same sets of fields but now investigating the downward influence. Section 3d details a collection of different approaches used to search for signals of a downward influence between the stratosphere and the troposphere.

a. A Demonstration of MCA for Troposphere-Stratosphere Teleconnections

We first demonstrate that the total squared covariance as a function of lag is a suitable tool to pick out the time scales of teleconnections between the wintertime stratosphere and troposphere. Sea level pressure anomalies have been shown to precede major disruptions of the stratospheric polar vortex (Kolstad et al. 2010; Cohen and Jones 2011; Mitchell et al. 2013; Lehtonen and Karpechko 2016; Domeisen et al. 2020). The vertical component of Eliassen-Palm (EP) flux is know to be a useful diagnostic for upward wave propagation (Palmer 1981; Esler and Scott 2005; Dunn-Sigouin and Shaw 2015; Jucker and Reichler 2018). We therefore begin by confirming the covariance between the two in Figure 1. For EP fluxes in the stratosphere (at 10, 30, and 100 hPa), sea level pressure tends to lead EP flux by 2–9 days, while there is negligible lead or lag between sea level pressure and EP fluxes in the troposphere (at 300 and 500 hPa). Previous studies have identified a time scale of 5–10 days for vertical propagation of planetary-scale waves from the surface to the 10

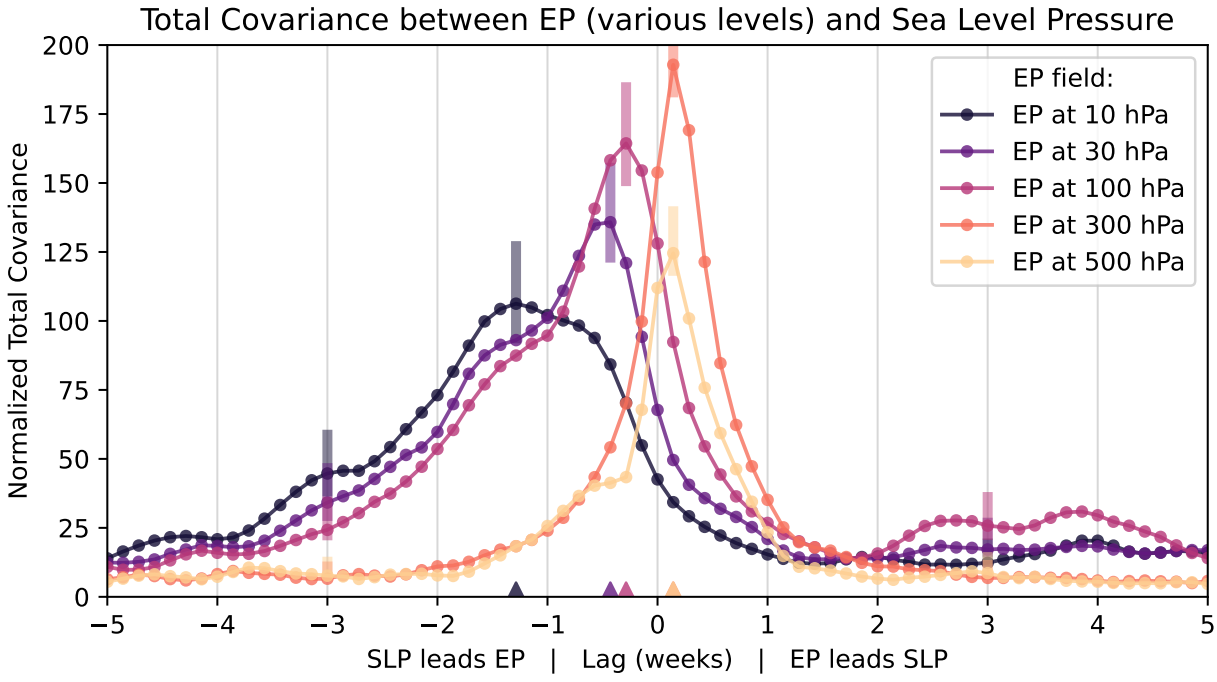

FIG. 1. **Peaks in total squared covariance pick out timescales of covariance.** The total squared covariance between sea level pressure (SLP) and the vertical component of Eliassen-Palm flux at multiple pressure levels (EP) as a function of the time lag between the surface and the stratosphere in weeks. Colored triangles along the bottom show the locations of the maxima (300 and 500 hPa overlap in this case) while shaded vertical bars denote 90% bootstrapped confidence intervals. Each curve is normalized according to Equation 3.

hPa level using observations (Hirota and Sato 1969; Perlwitz and Harnik 2003, 2004), correlations of time-lagged model output (Randel 1987; Christiansen 2001), and ray-tracing theory (Karoly and Hoskins 1982; Harnik 2002), which is in good agreement with our results. Both the lag and magnitude of maximal covariance also shift in a way that is consistent with upward propagation: the longest optimal lag and smallest maximal covariance occurs between the surface and 10 hPa, which are the furthest apart in space, and the lag shortens even as the covariance grows as we consider EP fluxes closer to the surface. EP flux at 500 hPa is an exception, as its covariance with the surface is smaller than at 300 hPa, but this could be due to the effect of increased noise from synoptic activity on the normalization (see Equation 3).

The asymmetry about the peaks for 10, 30, and 100 hPa may be indicative of two distinct timescales of upward propagation. The overall peak at −9 days at 10 hPa (black line) is echoed

by a shoulder in both 30 and 100 hPa around the same lag (purple and pink lines). Similarly, the overall peak at −2 days for 100 hPa and −3 days for 30 hPa also appears around −5 days at 10 hPa. A shoulder may represent a secondary peak superimposed on the larger one. These two superimposed peaks could indicate two processes with distinct timescales of upward propagation, one with a longer timescale of 9 days that dominates at 10 hPa and another with a shorter timescale of about 3 days that dominates in the lower stratosphere. With the total covariance alone, it is difficult to determine whether the two peaks correspond to distinct behaviors of the system, but the MCA analysis that follows will provide the corresponding patterns at the surface and in the stratosphere that will allow us to look for a change between −9 days and −3 days at each of the EP flux levels.

We follow up with MCA to identify the spatial patterns at the surface and in the stratosphere responsible for the covariance during upward propagation. Figure 2 shows the first two modes produced by MCA between the sea level pressure and EP at 10 hPa with a time lag of −9 days, the optimal lag corresponding to the largest covariance between these two fields in Figure 1. Mode 1 corresponds to a strengthening and slight northward shift of the climatological peak in EP flux centered at 65°N (Fig. 2b) and a sea level pressure dipole with one pole over Alaska and the other over Western Russia (Fig. 2e). The sea level pressure pattern of mode 1 is consistent with a documented precursor to SSWs (Kolstad et al. 2010; Lehtonen and Karpechko 2016; Domeisen et al. 2020), with a low over Alaska and the North Pacific and a high over Western Russia, which increases our confidence that MCA is able to capture established modes of covariability between the surface and the stratosphere.

Mode 1 accounts for the overwhelming majority, 91%, of the covariance between sea level pressure and vertical EP flux at 10 hPa. But while the stratospheric part of this mode also corresponds to the lion's share of the variance within EP flux at 10 hPa (83%), the surface component accounts for only 9% of the variance in the surface. We conclude that the sea level pressure precursor pattern described by mode 1 is less frequent and/or of smaller amplitude than other patterns of tropospheric variability. Even so, it corresponds to a strengthening of the EP10 peak at 65°N that accounts for most of the variability in the stratosphere. Mode 2 (Figure 2c,f), which accounts for only 8% of the covariance between sea level pressure and EP10, corresponds to a north/south shift of the EP10 maximum and resembles the Northern Annular Mode (NAM) or

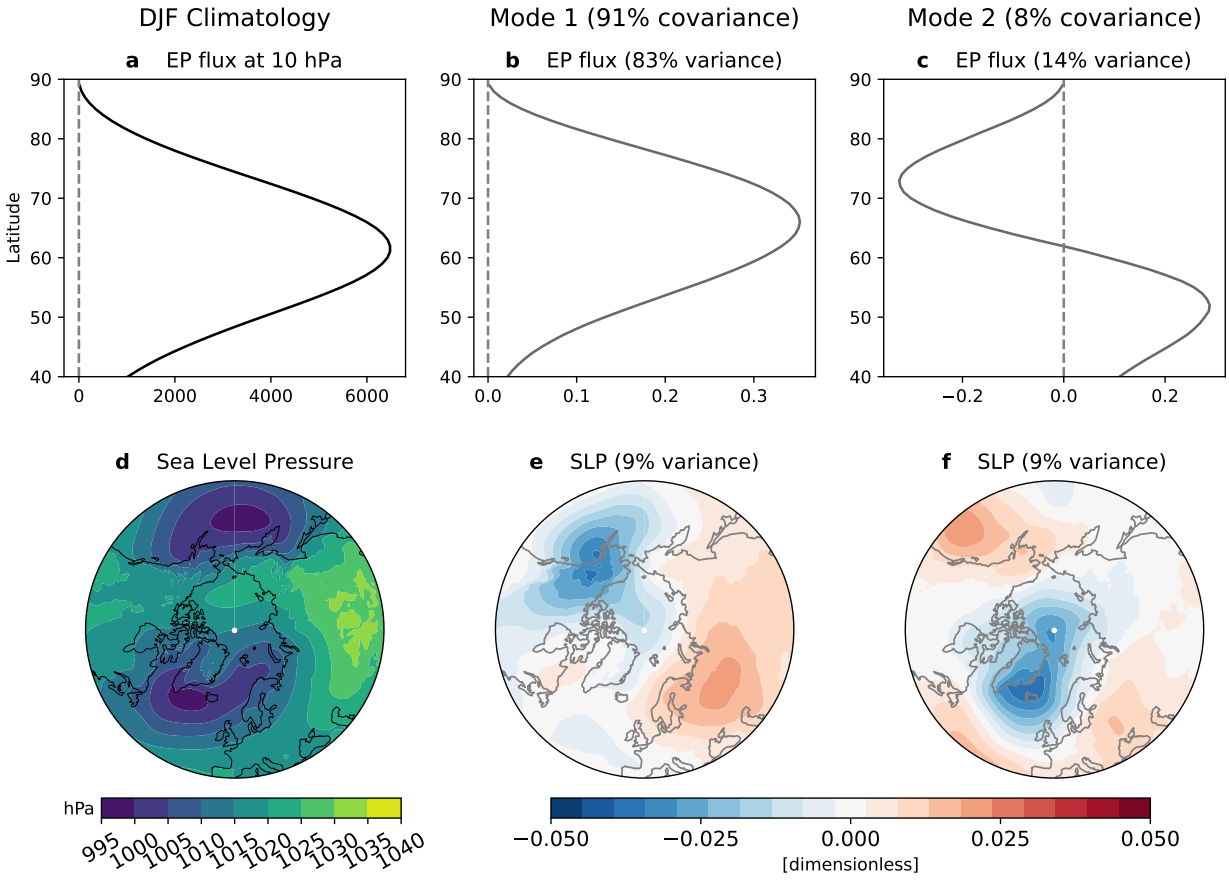

FIG. 2. **MCA identifies a known mode of covariance between the surface and stratosphere.** The climatology and first two MCA modes for EP at 10 hPa (a–c) and sea level pressure (d–f) at a time lag of −9 days (surface precedes stratosphere), corresponding to the time of maximum total covariance in Figure 1. The percent of the total covariance that is explained by each mode (Equation 5) is shown in parentheses at the top, while the percent of the variance in a specific field explained by the corresponding pattern for that mode (Equation 6) is shown above each subplot.

North Atlantic Oscillation at the surface (Wallace 2000; Baldwin 2001; Thompson et al. 2003) with poles over the Icelandic Low and the North Atlantic. It is interesting to note that mode 2 becomes more important at lower stratospheric levels, as both the covariance and stratospheric variance that it explains increase to 12% and 22% respectively by 100 hPa while the patterns remain the same.

By evaluating if and how the dominant mode patterns change as a function of lag, we can further determine whether the two peaks that appear at negative lags for 10, 30, and 100 hPa EP flux in Figure 1 correspond to distinct surface precursors. Figure 3 compares the first mode for EP at 30

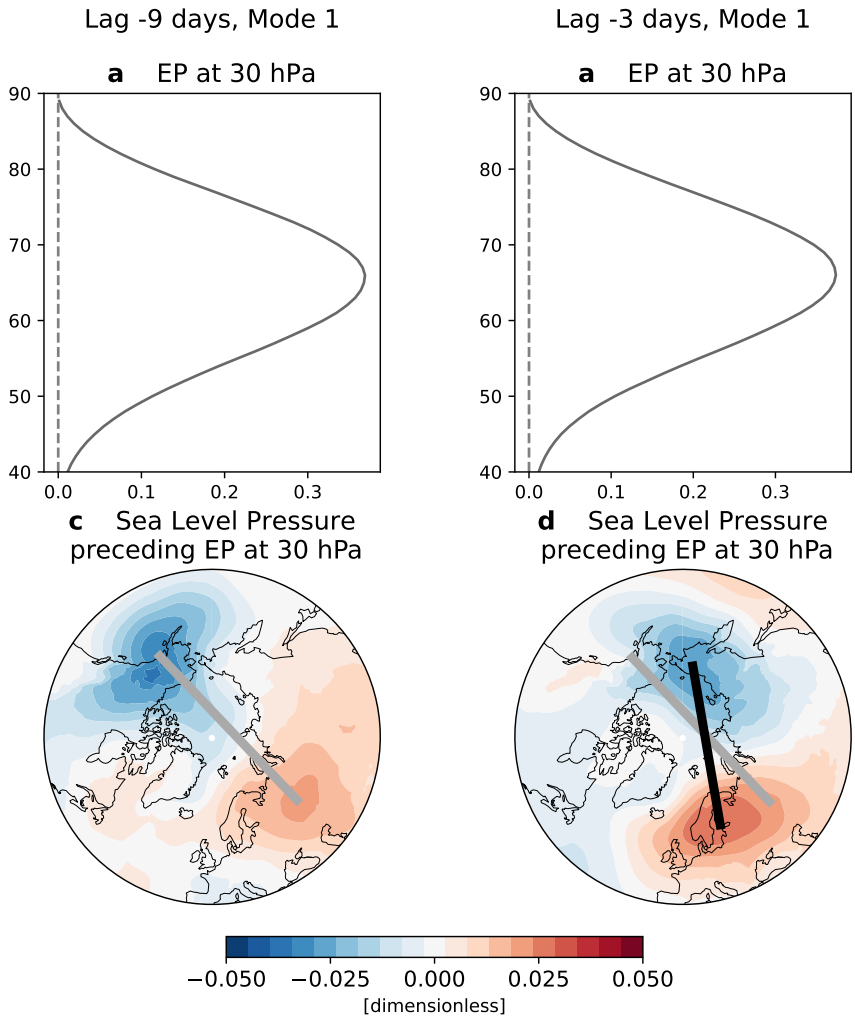

FIG. 3. **Rotation of sea level pressure precursor coincides with two distinct timescales of upward propagation.** First MCA mode between EP at 30 hPa and sea level pressure at a lag of −9 days (a, c; corresponding to the first peak in Figure 1) and −3 days (b, d; corresponding to the second peak in Figure 1). The thick grey line in panel c connects the dipole centers and is repeated in panel d along with a black line connecting the new dipole centers to emphasize the rotation about the pole, which is roughly 60°.

hPa and sea level pressure, which accounts for over 85% of the covariance, between lag −9 days and lag −3 days, corresponding to the long and short upward propagation timescales identified above. There is a dipole in the sea level pressure anomaly at both lags, but it rotates about the pole by almost 60° from −9 to −3 days, moving from the eastern to the western side of the sea level pressure climatological low over the North Pacific (compare the orientation of the dipole in panel c vs d in Figure 2, illustrated by thick grey and black lines). The change in sea level pressure

precursor indicates that there are two major sea level pressure anomalies that are responsible for over 85% of the covariance with stratospheric vertical EP flux: a low over Alaska and a high north of the Caspian Sea precedes an enhancement of upward EP flux in the stratosphere by about 9 days (Figure 3c), while a low over Eastern Russia and a high over Northern Europe precedes an enhancement of upward EP flux in the stratosphere by about 3 days (Figure 3d). Dunn-Sigouin and Shaw (2015) also observed a rotation of a tropospheric wave-1 pattern over the course of about 10 days preceding anomalously strong upward wave propagation into the stratosphere, but over a larger angle than we identify here. The first mode in sea level pressure at these two lags looks nearly identical for EP at 10 and 100 hPa as it does for the 30 hPa level shown in the figure, increasing our confidence that the aligned peaks in Figure 2 represent the same wave signals manifesting at multiple levels in the stratosphere.

The two timescales of upward propagation that we detect in Figures 2 and 3 are broadly, but not entirely, consistent with vertical propagation of wave-1 and wave-2. With vertical propagation speeds of 5 km/day for wave-1 in the stratosphere and 7 km/day for wave-2, and half that in the troposphere, it would take 4–8 days for wave-1 and 2–4 days for wave-2 to get from the surface to 10 hPa (Hirota and Sato 1969; Karoly and Hoskins 1982; Randel 1987), which compare favorably to our detected lags of -9 days and -3 days. Covariability between the surface and the 10 hPa level is strongest for the longer timescale while the lower stratosphere is dominated by the shorter timescale, which is also consistent with the fact that wave-2 is less prone to propagate to higher levels. This suggests that the two sea level pressure anomalies in Figure 3 may be favorable for wave-1 vs wave-2 generation. However, when we move from the time scale to the structure of these teleconnections, the wavenumber distinction is less clear. The sea level pressure precursor does not have a clear wave-2 pattern for the -3 day lag (Figure 3d). EP flux is a zonal-average quantity, so we cannot look for wave structure as easily there, but we do note that the rotation of the sea level pressure anomaly does not show up when passing from -9 to -3 days' lag for PV at 10, 30, or 100 hPa and sea level pressure (Figure S3 in the supplementary material has the first two modes for PV10 at weekly lag resolution, but even at daily resolution the rotation of the sea level pressure dipole does not appear). The first and second modes of PV at 100 hPa and sea level pressure show higher-order wave patterns in the stratosphere that may indicate the presence of wave-2, but the

corresponding surface patterns do not show either a wave-2 structure or the rotation we identified in the EP flux precursors.

b. Characterizing the upward influence

In expanding our analysis to a wide variety of both stratospheric and tropospheric fields, we find that lags from a few days up to one week in the upward direction maximize the total covariance in almost all cases. We consider several stratospheric fields at 10 hPa, including potential vorticity (PV), zonal wind (U) and the vertical component of EP flux (EP), alongside several tropospheric fields including daily minimum surface temperature (T_{min}), sea level pressure (SLP), and the 500 hPa geopotential height (Z500). Figure 4 of the total covariance between stratospheric fields PV10, U10, and EP10 and tropospheric fields T_{min}, SLP, and Z500 shows maximum total covariance at negative lags and insignificant covariance at positive lags for almost all pairs of tropospheric and stratospheric fields. Naively, one would expect upward propagation to result in a peak at negative lags (troposphere leads stratosphere) and downward propagation to result in a peak at positive lags (troposphere lags stratosphere). Indeed, the 3–4 day time scale for upward propagation that we find between 500 hPa and 10 hPa (peaks in brown lines in Figure 4) is in excellent agreement with previous results of 3–5 days (Perlwitz and Harnik 2003, 2004; Shaw et al. 2010), but we find no such peak indicating downward influence. These results, therefore, detect upward but not downward propagation.

Now that we have expanded our consideration to all stratospheric fields, the particular significance of the sea level pressure precursor that we identified in Figure 2 is reinforced. Figure 5 shows the patterns corresponding to the first MCA mode across three different stratospheric fields at 10 hPa, all analyzed for their covariance with sea level pressure, with a lag of -1 week. The sea level pressure pattern is nearly identical across all three stratospheric fields, with slight variations in the location of the pole over Eurasia. This mode indicates that a low pressure anomaly over Alaska and a high over western Russia at the surface tend to be followed a week later by: a shift of the stratospheric vortex into the sector over western Russia (Figure 5a); a clockwise circulation anomaly over western Russia and a counterclockwise anomaly over northwestern Canada in the stratosphere (Figure 5b); and a strengthening of the climatological peak in EP10 (Figure 5c). While there are previous studies that have identified this sea level pressure pattern as a precursor to SSWs (Kolstad

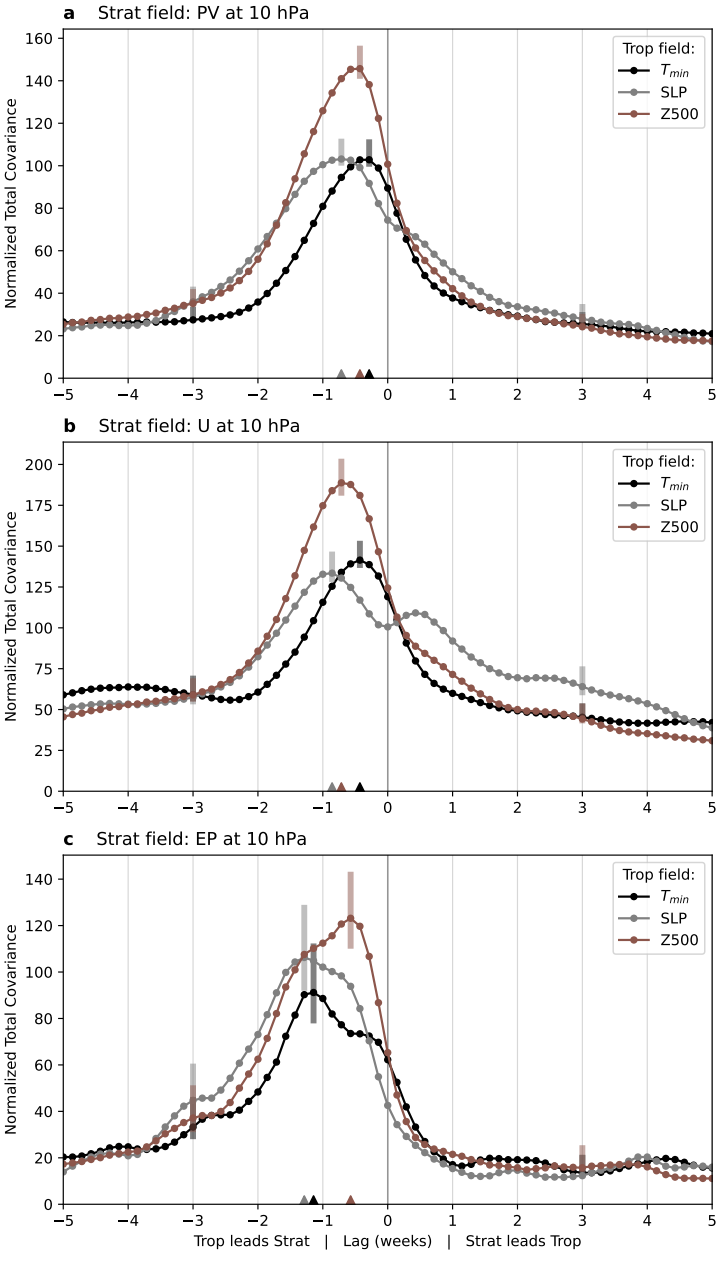

FIG. 4. **Covariance between multiple stratosphere-troposphere field pairs shows evidence for upward but not downward propagation.** Total covariance between a stratospheric field at 10 hPa (PV (a), U (b) or EP flux (c)) and a tropospheric field (daily minimum surface temperature (black), sea level pressure (grey), or 500 hPa geopotential height (brown)) as a function of the lag in weeks between the two fields. Colored triangles along the bottom show the locations of the maxima while shaded vertical bars denote 90% bootstrapped confidence intervals. Each curve is normalized according to Equation 3.

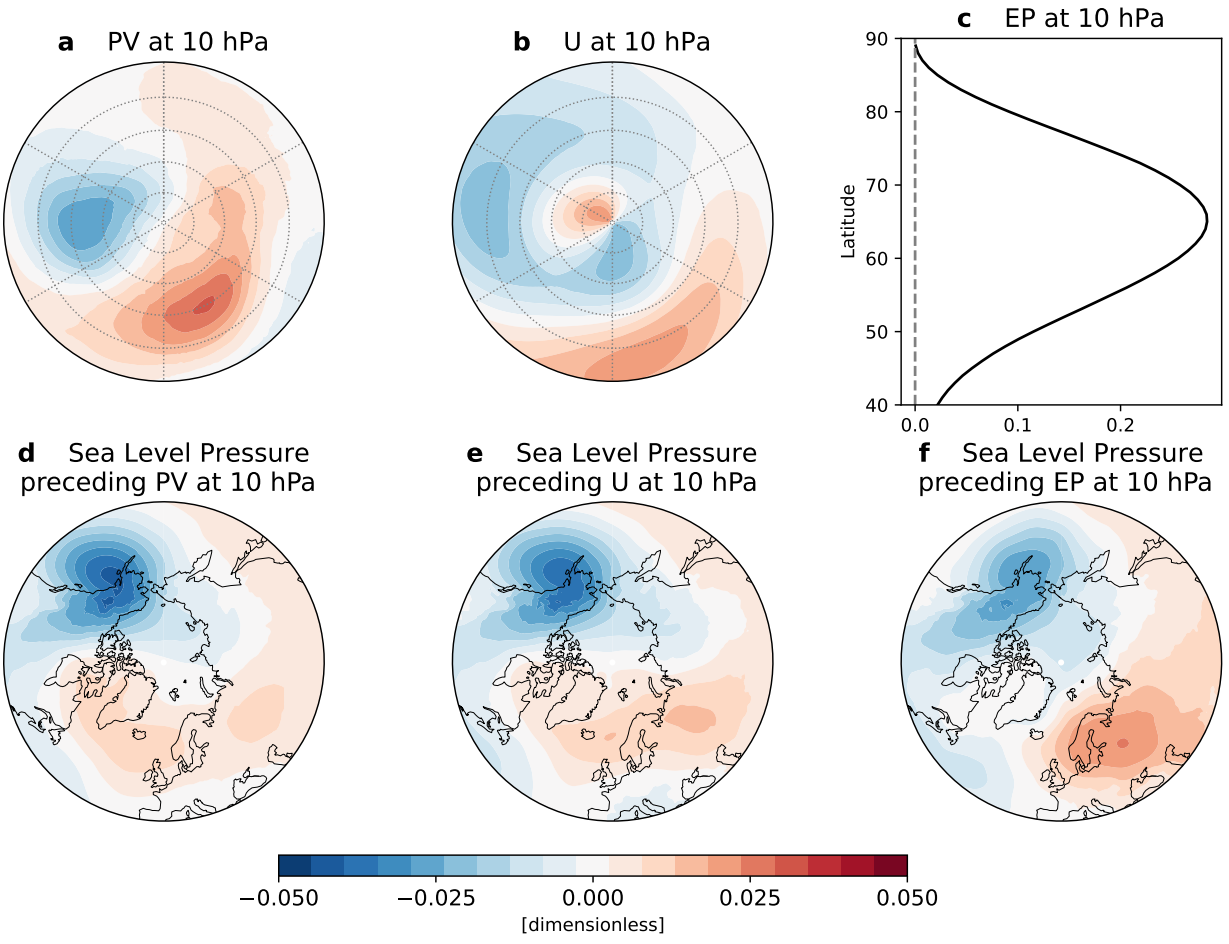

FIG. 5. **The sea level pressure anomaly that leads the stratosphere by one week is similar across different stratospheric fields and is not either the NAO or NAM/AO.** The first MCA mode between a stratospheric field at 10 hPa (PV (a), U (b), or EP flux (c)) and sea level pressure (d–f) at a lag of −1 week.

et al. 2010; Lehtonen and Karpechko 2016; Domeisen et al. 2020), there are others that have found a different pattern to be more prominent (Martius et al. 2009; Kolstad et al. 2010; Mitchell et al. 2013). As our MCA analysis is not restricted to SSWs but instead considers covariance over the entire winter, one explanation for this disagreement is that the sea level pressure precursor we and others have identified is not limited to SSWs but instead describes a more general mode of covariability between the surface and the stratosphere. Based on the time scale of about one week and the discussion above concerning the source of the two peaks in EP and SLP from Figure 1, it is likely that the surface precursor and stratospheric response in Figure 5 is characteristic of a wave-1 disturbance.

c. Characterizing the downward influence

Looking back at the total covariance over all combinations of fields in Figure 4, we now consider the possibility of a downward influence. While all pairs of fields peak at negative lags, consistent with upward propagation, U10 (and, to a lesser extent, PV10) and sea level pressure has a secondary peak when the surface lags the stratosphere by +3 days (Figure 4b). Previous studies have identified downward propagation of zonal-mean zonal wind anomalies in the wintertime stratosphere (Kuroda and Kodera 1999; Christiansen 2001; Perlwitz and Harnik 2004; Shaw et al. 2010), but over longer timescales of a few weeks rather than the 3 days indicated by the second peak in Figure 4b (grey line). One way to get a faster response than the wave-mean flow interaction (the downward progression of zonal-mean zonal wind deceleration) is through a mass redistribution over the polar cap, which affects sea level pressure (described in section 1; Hartley et al. 1998; Ambaum and Hoskins 2002; Black 2002). If we compare the MCA mode patterns for U10 and sea level pressure at the two peaks in covariance, −6 days and +3 days (see Figure S1 in the supplementary material), we do observe an overall strengthening of the zonal wind at high latitude preceding a decrease in sea level pressure over the pole 3 days later. PV at 10 hPa and sea level pressure at +3 days is also consistent with this explanation, where the first mode is characterized by a high PV anomaly followed by a low sea level pressure anomaly over the pole (not shown).

Much of the interest in downward propagation in the literature is concerned with the response of temperature extremes to stratospheric disruption, as such a connection could be used to improve weather prediction lead times. However, we find little indication of a downward influence between any of our stratospheric fields and the daily minimum temperature T_{min}, realized as a peak in the total squared covariance at a positive lag. Instead, T_{min} tends to lead all stratospheric fields by a few days (covariance peaks at negative lags in Figure 4). The dynamical mechanism of surface temperatures preceding stratospheric variance is likely that sea level pressure, which has the largest lead time of any tropospheric field considered, is related to upward propagation while T_{min} responds to the surface pressure anomalies a few days later. The response of T_{min} to sea level pressure anomalies would, therefore, lead to an apparent short delay between temperature anomalies and stratospheric variability. Indeed, we find that the pattern of T_{min} for mode 1 is consistent with the geostrophic circulation anomalies that would be induced by the sea level pressure anomalies for mode 1, with northward (warm) advection over Canada and southward (cold) over eastern Russia (see Figure S2

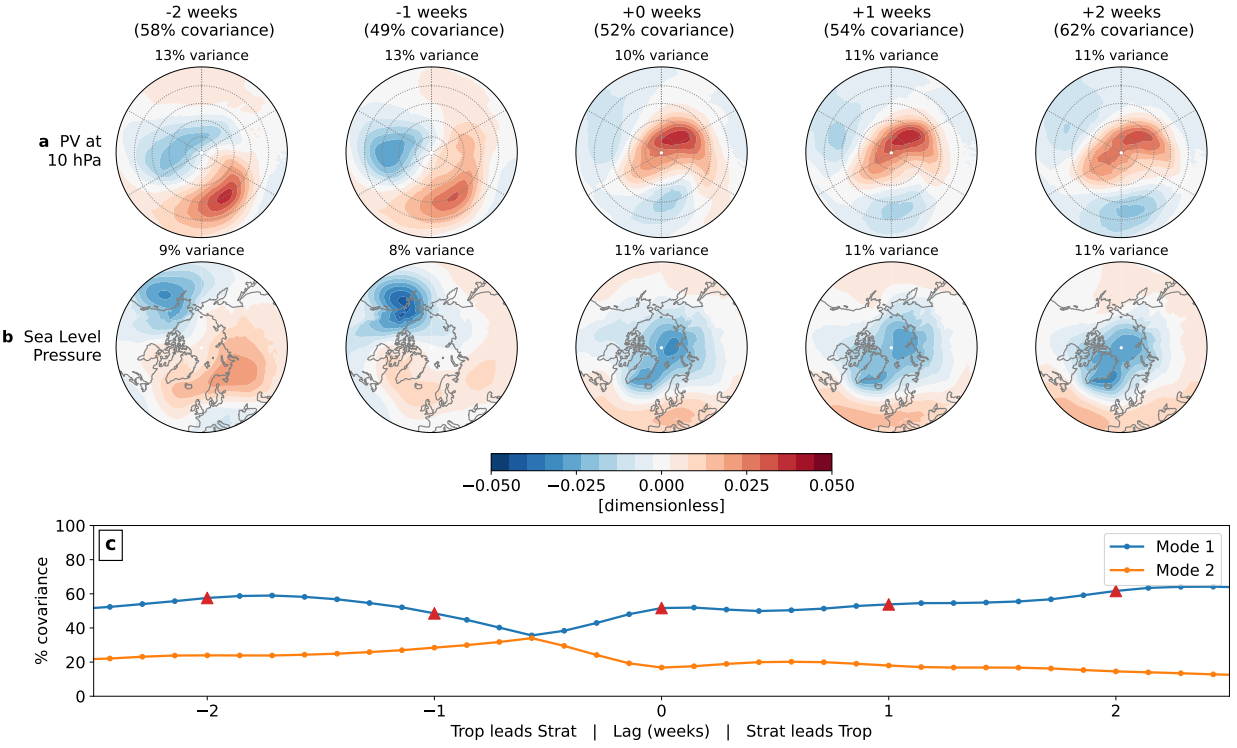

488 FIG. 6. **The structure of the first MCA mode changes near lag zero.** The mode pattern that maximizes
489 covariance between PV at 10 hPa (a) and the sea level pressure (b) for five different lags ranging from −2 weeks to
490 +2 weeks. (c) The percent of the total covariance explained by the first two modes, with red triangles to indicate
491 the mode patterns depicted above. The two modes are exchanged at a lag of −4 days, as shown in Figure S3 of
492 the supplementary materials.

485 in the supplementary material). The downward response of sea level pressure identified above
486 following U10 and PV10, which is consistent with the redistribution of mass over the polar cap,
487 does not appear to produce an appreciable signal in temperature extremes.

493 We can also consider how the spatial structure of the first mode changes when shifting from
494 upward to downward lags, as illustrated in Figure 6. A major shift occurs between a lag of −1
495 week and no lag: the dominant mode we identified in Figure 5 is supplanted by a pattern much
496 more reminiscent of the NAM in sea level pressure. From Figure 6c, we can see that the first
497 mode pattern changes because it is replaced by what was the second mode at a lag of −4 days,
498 where the two modes explain a comparable percentage of the covariance between the two fields;
499 see Figure S3 in the supplementary materials for the mode patterns of the first and second modes

across this transition. The NAM-like mode also persists over a large range of lags; the sea level pressure pattern that most closely covaries with PV10 at no lag also tends to lag it by +1 and even +2 weeks.

We have argued that the mode patterns at a lag of -1 week indicate upward propagation due to the corresponding peak in the total covariance at that negative lag. But if the pattern appearing at zero and positive lags in Figure 6 has a peak in the total covariance that is expressed by the shoulder on the gray curve in Figure 4a, it seems to be a weak one. Our identification of a NAM-like pattern at the surface for positive lags is consistent with other studies that have found that a negative NAM signal at the surface tends to follow SSWs in observations (Baldwin and Dunkerton 2001; Charlton and Polvani 2007; Mitchell et al. 2013) and models (Tomassini et al. 2012; Sigmond et al. 2013; Hitchcock and Simpson 2014; White et al. 2020). However, the decrease in the total covariance as the lag increases from zero (Figure 4a) leads us to suspect that the NAM-like pattern at the surface tends to co-occur with stratospheric variability rather than lag it. There are at least two explanations for the persistence of the mode 1 (NAM-like) pattern over positive lags observed in Figure 6 for both PV and SLP. One possibility is that there is a continuous dynamical teleconnection between the stratosphere and troposphere over several weeks. Another possibility is that there is a short-lived dynamical teleconnection, with a lag of $0-3$ days, that produces features at the stratosphere and surface that tend to persist independently for several weeks. Since the total covariance tends to decrease continuously at positive lags (grey line in Figure 4a), we find the second possibility more likely, that the teleconnection itself may be short-lived but the surface and stratospheric anomalies tend to persist once formed.

We further note that subtracting the PV anomaly of mode 1 at positive lags (Figure 6) from the climatology results in a pattern that is consistent with a split-type SSW, placing daughter vortices over Northern Europe and western Canada (see the left column of Figure S4 in the supplementary materials for a visualization). Doing the same with the sea level pressure anomaly of the same mode gives an increase in sea level pressure over the pole, consistent with the negative phase of the NAM. Mitchell et al. (2013) found that split events led to a negative NAM signal at the surface where displacement-type SSWs did not. Figure 6 and the above discussion imply that composites following split-type SSWs may pick out a NAM-like signal in sea level pressure because it co-

occurs with the SSW or lags by just a few days and then persists for a few weeks rather than because it is a result of long timescales of downward influence.

d. The Search for Downward Propagation

Given that the MCA analysis above did not identify a clear signal of downward propagation, particularly on the weekly and longer timescales generally discussed in previous studies, we next pursue a series of more targeted searches for a downward influence that are laid out in this section. First, composites of the vertical component of anomalous EP flux relative to SSW onset are presented in part 1. Motivated by those results, part 2 conducts an MCA analysis on EP fields that have been masked to preserve only upward or downward fluxes. Finally, part 3 searches for the signature of wave-mean flow interaction by targeting the zonal-mean zonal wind in the time period around SSWs.

1) Composites over SSWs

A downward influence from the stratosphere on the troposphere and potentially the surface is thought to occur primarily following SSWs, while so far we have analyzed the entire winter period. We, therefore, begin with a series of composites over all SSWs in our data set (identified from the zonal-mean zonal wind reversal criterion of Charlton and Polvani 2007) of the EP flux anomaly at various pressure levels in Figure 7. At 100 hPa, there is a dramatic decline from positive to negative EP flux anomalies once the SSWs begin. This time, denoted $t = 0$ in the figure, corresponds to the minimum zonal-mean zonal wind at 60°N following each SSW and is marked by the vertical grey line in the plot. The downward EP flux anomaly persists all the way down to 500 hPa with increasing temporal variability but is confined largely north of 50°. We repeat this analysis but distinguishing between “reflecting" and “absorbing" SSWs according to Kodera et al. (2016) in Figure S5 of the supplementary materials; this sub-type classification makes surprisingly little difference in the downward signal for these EP flux anomaly composites.

This appears consistent with downward propagation over a few weeks following SSWs, but based on the total covariance in Figure 4 does not appear to translate to appreciable covariability with sea level pressure or daily minimum temperature. To reconcile these observations, we note that the EP flux anomalies in Figure 7 cannot distinguish between a decrease in upward flux and an increase

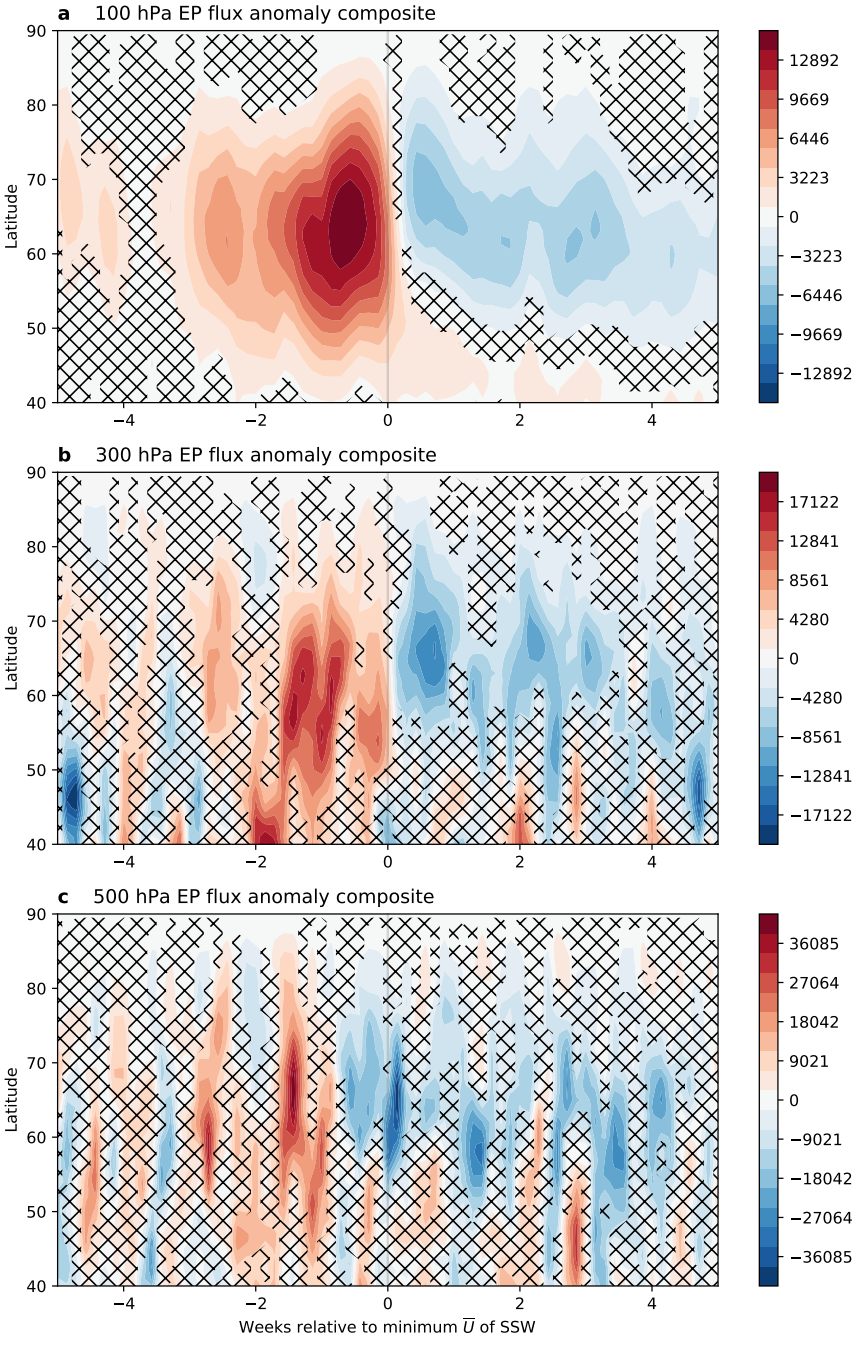

FIG. 7. **Downward EP flux anomalies appear to reach the mid-troposphere following SSWs.** Composites over all SSWs of the vertical EP flux anomaly from day-of-year climatology at 100 hPa (a), 300 hPa (b), and 500 hPa (c). The date of minimum zonal-mean zonal wind following SSW detection corresponds to zero along the x-axis and is indicated with a vertical grey line. Black hatches mask regions that are not significant at the 90% level (based on a two-sided test from the 5^{th} to 95^{th} percentile).

in downward flux. The observed transition in Figure 7 from positive to negative EP flux anomalies during SSWs could indicate the failure of planetary waves to continue to propagate upwards, a direct result of the brief reversal of the zonal wind that accompanies an SSW (Charney and Drazin 1961). But it could also indicate the presence of downward EP flux characteristic of a downward wave propagation (Kodera et al. 2016), which we are most interested in detecting, so in the next section we transition from EP flux anomalies to positive and negative absolute EP flux in our search for downward propagation.

2) Analyzing Upward and Downward EP Flux Separately

The suggestion that downward EP flux anomalies may reach as low as 500 hPa in the analysis above motivated us to see whether absolute upward and downward EP flux rather than just anomalies do the same. In this analysis, we compare two EP flux fields at different heights: one field is fixed at 100 hPa while the other varies between 10 hPa and 850 hPa. We first remove the linear trend over the entire data set and scale by the square root of latitude, and for this analysis, we do not subtract the seasonal cycle. We isolate the downward EP flux at all levels by masking out values greater than zero. For upward EP flux, we do the same but masking out values less than zero. We then proceed with calculating the total covariance between the two fields as described in section 2. To make sure that the total covariance is not dominated by a seasonal cycle, we inspected the expansion coefficients for the first three MCA modes to confirm that they do not express a seasonal cycle.

Figure 8 shows the covariance between upward (a) and downward (b) EP at 100 hPa and levels both above and below. There is evidence of upward propagation in Figure 8a: higher levels tend to lead EP at 100 hPa (brown lines peak at positive lags) while lower levels tend to lag (purple lines peak at negative lags). The magnitude of maximum covariance varies with the vertical separation between the two fields (paler shades have a higher magnitude than darker shades of the same color). Noting that the peak for EP at 850 hPa occurs about 5 days before the peak for 10 hPa, one might conclude that it takes about 5 days for upward EP flux anomalies to be communicated between 850 and 10 hPa. This time scale is consistent with Dunn-Sigouin and Shaw (2015), who found a lag of 5–10 days between heat flux anomalies in the mid-troposphere and the 10 hPa level during upward wave propagation.

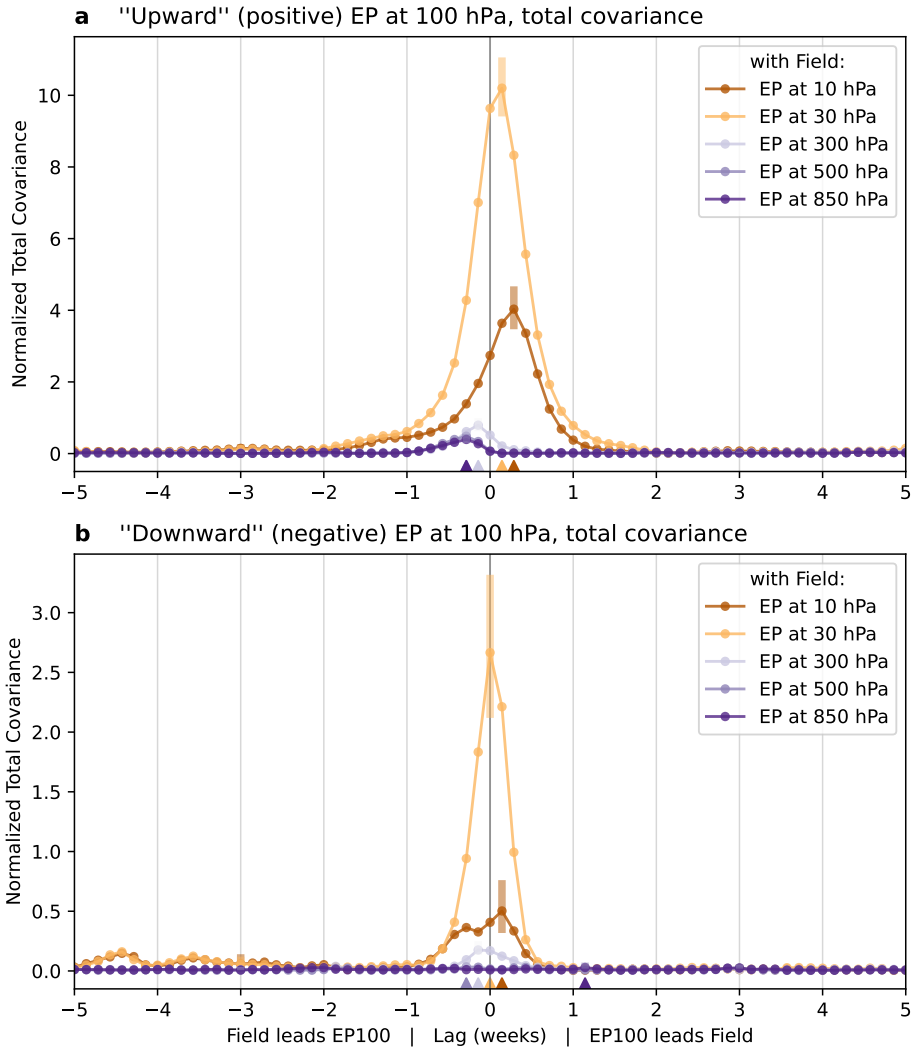

570 FIG. 8. **A separate analysis of upward and downward EP flux shows signal of upward but not downward**
571 **propagation.** Total covariance between "upward" (negative EP flux) or "downward" (positive) EP flux at 100
572 hPa and at various levels throughout the troposphere and stratosphere. Brown lines correspond to levels above
573 EP100 while purple indicates levels below EP100. Colored triangles along the bottom show the locations of
574 the maxima (some may overlap) while shaded vertical bars denote 90% bootstrapped confidence intervals. Each
575 curve is normalized according to Equation 3.

597 Downward propagation is not as evident in Figure 8b. For downward propagation, we would
598 expect each curve to peak in the reverse order with respect to lag that they did for upward EP: 10
599 and 30 hPa would peak at negative lags and 300, 500 and 850 hPa at positive lags. Instead, there
600 are peaks at both positive and negative lags for 10, 30, and 300 hPa while 500 and 850 hPa have

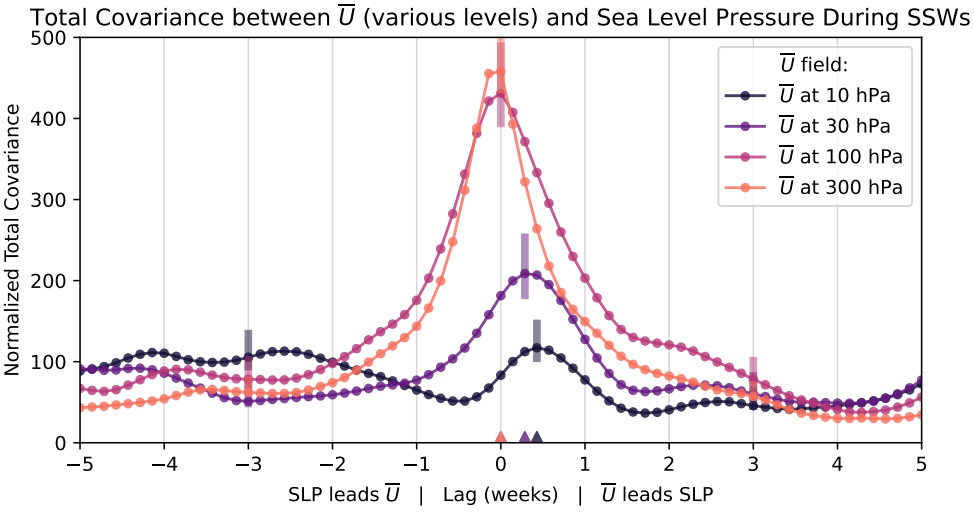

FIG. 9. **Sea level pressure lags zonal-mean zonal wind by just a few days during SSWs.** Total squared covariance between zonal-mean zonal wind at 10, 30, 100, and 300 hPa and sea level pressure, where the zonal-mean zonal wind field spans the period from two weeks before to six weeks after SSW onset for all SSWs in the dataset. Colored triangles along the bottom show the locations of the maxima (100 hPa and 300 hPa overlap in this case) while shaded vertical bars denote 90% bootstrapped confidence intervals. Each curve is normalized according to Equation 3.

no peaks distinguishable from the noise. Perhaps our dataset is insufficiently long for identifying downward propagation of EP flux. It is also possible that many downward propagation events co-occur with upward wave forcing and so the overall sign of the EP flux is not able to disentangle the two.

3) Zonal-mean Zonal Wind During SSWs

Previous work has suggested that SSWs are responsible for a significant downward influence on surface weather. To look for a downward influence related to these events, we now restrict our analysis to only those times corresponding to SSWs. We first identify all major SSWs between 1959 and 2020 in the ERA5 dataset using the zonal-mean zonal wind at 60°N criterion of Charlton and Polvani (2007). For each SSW, we restrict the stratospheric field to span from 2 weeks before to 6 weeks after SSW onset, then apply a lag relative to that 8-week window to get a corresponding tropospheric time series. By combining these 8-week windows for all SSWs, we produce new timeseries that can be used to calculate the total covariance between the troposphere

and stratosphere focused on the period spanning SSWs. Note that the same processing was applied to each data set before selecting out the SSWs as was described in section 2: at each grid point, we apply area-weighting, remove the linear trend, and subtract off the seasonal cycle.

The large magnitude of the disruption to the stratospheric vortex during SSWs suggests that these events would be optimal times to look for a downward influence. Based on the wave-mean flow interaction picture for downward propagation, whereby a succession of upward-propagating waves moves a deceleration of the zonal jet downward within the stratosphere, we would expect to see a downward signal in the zonal mean zonal velocity. But even when our analysis is restricted to the period around SSWs, the downward influence detected between the zonal-mean zonal wind and sea level pressure (Figure 9) spans just a few days rather than the weeks suggested by previous studies (Baldwin and Dunkerton 2001; Mitchell et al. 2013; Sigmond et al. 2013; Hitchcock and Simpson 2014). The downward peak at +3 days also does not appear to persist below 30 hPa. The upward peak that was present at -6 days in U10 and sea level pressure in Figure 4b has disappeared in the zonal-mean $\overline{U10}$ and sea level pressure in Figure 9, suggesting that upward propagation during and after SSWs appears in the zonal wind but not in the zonal-mean zonal wind. The first mode at +3 days (not shown) indicates that a deceleration of the zonal wind at 10 and 30 hPa tends to precede the negative phase of the NAM, consistent with the full zonal wind results (see Figure S1 in the supplementary material) and previous findings of the surface response to SSWs (Baldwin and Dunkerton 2001; Mitchell et al. 2013; Sigmond et al. 2013; Hitchcock and Simpson 2014). However, given the rapid decline of the total covariance after the peak for $\overline{U10}$ and $\overline{U30}$ in Figure 9, the sea level pressure response does not appear to operate on time scales longer than a week or two. Perhaps eddy feedbacks or coupling to sea surface temperatures could prolong the timescale of tropospheric response beyond that of the pressure field alone (Wittman et al. 2004; Lubis et al. 2016), but then it is surprising that we do not see evidence of such longer downward timescales showing up in minimum temperatures in Figure 4b (T_{min}, black line).

4. Conclusions

We set out to identify time lags and spatial patterns most relevant to covariance between the troposphere and stratosphere in Northern Hemisphere winter. One of the aims was to identify the signal of both upward and downward propagation. We consider the total covariance as a function

of the time lag between a set of tropospheric and stratospheric fields in daily ERA5 reanalysis spanning 61 years. While we find evidence of an upward influence with time lags of about 3–9 days, we could not find a signal of a downward influence over time scales longer than 3 days using our analysis approach. The covariance between the troposphere and stratosphere is maximized when the tropospheric field leads the 10 hPa field by up to 9 days (with a shorter lag when the same tropospheric field is paired with a lower stratospheric field). A lag in the upward influence of up to 10 days is in good agreement with previous studies, which have identified an upward wave propagation speed of roughly 5 km/day (Hirota and Sato 1969; Karoly and Hoskins 1982; Randel 1987) and a corresponding time scale of 3–10 days (depending on the zonal wavenumber) between the surface and the 10 hPa level (Christiansen 2001; Perlwitz and Harnik 2003). At the optimal time lag, we employ Maximum Covariance Analysis to identify the spatial patterns that account for the covariance between the two fields. This allows us to identify two sea level pressure patterns that account for the majority of the time-lagged covariance in the EP flux, a measure of wave activity: a low over Alaska and a high north of the Caspian Sea precedes an enhancement of upward EP flux in the stratosphere by about 9 days (Figure 3c), while a low over Eastern Russia and a high over Northern Europe precedes an enhancement of upward EP flux in the stratosphere by about 3 days (Figure 3d). The first pattern, which has a longer time scale and may correspond to wave-1, was also found to maximize the covariance between sea level pressure and stratospheric PV and zonal wind fields. Some studies have identified a similar pattern as a precursor to SSWs (Kolstad et al. 2010; Lehtonen and Karpechko 2016; Domeisen et al. 2020), although it is unclear why this specific pattern is most favorable for wave generation and stratospheric vortex disruptions. The structure of our identified sea level pressure precursor is not, for example, aligned with that of climatology. Such an alignment with the climatology for the 500 hPa geopotential height, for example, has been suggested as a potential mechanism for enhancing upward wave activity (Garfinkel et al. 2010; Smith and Kushner 2012).

Our analysis brings up new questions about the nature of upward and downward influence that remain to be explored. First is the possibility of two distinct timescales of upward wave propagation. We identify maxima in the covariance between sea level pressure and stratospheric EP flux at lags of both -9 days and -3 days. These time scales are consistent with previous work on the upward propagation speed of wave-1 vs wave-2 (Hirota and Sato 1969; Karoly and Hoskins 1982; Randel

1987; Perlwitz and Harnik 2003, 2004; Shaw et al. 2010), but we do not see those wave structures clearly at the surface or in the stratosphere in this analysis. The rotation of the sea level pressure anomaly about the pole which precedes stratospheric EP flux anomalies at the shorter timescale is furthermore not observed in the mode patterns for any of the other stratospheric fields analyzed here. That being said, the mode patterns change with unusual rapidity within a few days of zero lag as there arise multiple patterns responsible for comparable proportions of the total covariance, making it difficult to rule out the possibility that such a rotation of the surface anomaly precedes some wave-1 or wave-2 pattern in the stratosphere. It is also possible that the shorter timescale represents a straightforward upward wave propagation while the longer timescale arises from some feedback that enhances and alters the wave behavior at higher levels; investigating this possibility is outside the scope of this work but could prove fruitful. The second question concerns the somewhat conflicting evidence of a downward influence. When restricted to the period around SSWs, we found some indications of downward influence in EP flux anomalies (Figure 7) and in zonal-mean zonal wind (Figure 9), but the full winter analysis found no influence on surface temperatures (Figure 4). Wave reflection proved much more difficult to detect with this method (see discussion for Figure 8), but previous studies suggest that it should appear even without SSWs in reflective winters (Perlwitz and Harnik 2003; Kodera et al. 2016). We leave a more targeted search either excluding SSWs or under reflective vs non-reflective conditions to future work.

A number of caveats are important to keep in mind when interpreting these results. Reanalysis data can be noisy for some fields due to short term variability. The time record of 61 winters is also somewhat short, particularly relative to the size of the spatial dimension (fields defined on a latitude-longitude grid have 18,000 spatial points compared to around 5,500 time points) and especially when limiting our analysis to times with positive or negative values only as in the upward and downward EP flux analysis in section 3d2. While it is common practice to use SVD on datasets with more spatial samples than temporal samples, the cross-covariance matrices that result are an approximation (Bretherton et al. 1992). In addition, the mode patterns identified with MCA are symmetric with respect to sign, such that the mode pattern represented by the vectors $\mathbf{u}_k$, $\mathbf{v}_k$ necessarily implies a covariance between $-\mathbf{u}_k$ and $-\mathbf{v}_k$ as well. This may not be a desirable feature if the processes regulating covariance between the troposphere and stratosphere are not symmetric in this way.

Unlike many studies of stratosphere-troposphere teleconnections, our analysis is applied to the entire record rather than restricted to the times around SSWs. It has still been convenient to compare our identified mode patterns (Figures 2, 3, 5, 6) to patterns described in the literature on SSW precursors because they have been widely studied. Yet the fact that the sea level pressure pattern that we found to precede stratospheric variability matches the literature in some (Kolstad et al. 2010; Lehtonen and Karpechko 2016; Domeisen et al. 2020) but not all (Cohen and Jones 2011; Mitchell et al. 2013) cases may indicate that this is a stratosphere-troposphere teleconnection mode that includes but is not limited to SSWs. The expansion coefficients for the first and second MCA modes, indicating the strength of those modes at a given point in time, might serve as an index for coupling strength between the troposphere and stratosphere that avoids the ambiguities of identifying and classifying SSWs. Future work could determine the extent to which the mode patterns identified in Figure 5 describe non-SSW teleconnections at work between the troposphere and the stratosphere in Northern Hemisphere winter.

Acknowledgments. We thank Mathew Barlow and Laurie Agel for very helpful discussions. This work was funded by the U.S. Department of Energy (DOE) Office of Science Biological and Environmental Research grant DE-SC0023134. KH was funded by a National Defense Science and Engineering Graduate (NDSEG) Fellowship. ET thanks the Weizmann Institute for its hospitality during parts of this work. We would like to acknowledge high-performance computing support from Cheyenne and Casper (doi:10.5065/D6RX99HX) provided by NCAR's Computational and Information Systems Laboratory, sponsored by the National Science Foundation.

Data availability statement. Reanalysis output for ERA5 is available at no cost through the Copernicus Climate Data Store at `https://cds.climate.copernicus.eu`. EP fluxes were calculated using Equation 1 in the text and following the procedure at `http://www.met.reading.ac.uk/~pn904784/snap/ep_flux_calculations.html`.

References

Albers, J. R., M. Newman, A. Hoell, M. L. Breeden, Y. Wang, and J. Lou, 2022: The February 2021 Cold Air Outbreak in the United States: a Subseasonal Forecast of Opportunity. *Bulletin of the American Meteorological Society*, **-1 (aop)**, https://doi.org/10.1175/BAMS-D-21-0266.1.

Ambaum, M. H. P., and B. J. Hoskins, 2002: The NAO Troposphere–Stratosphere Connection. *Journal of Climate*, **15 (14)**, 1969–1978.

Andrews, D., J. Holton, and C. Leovy, 1987: *Middle Atmosphere Dynamics*. Academic Press, 489 pp.

Ayarzagüena, B., and Coauthors, 2018: No robust evidence of future changes in major stratospheric sudden warmings: a multi-model assessment from CCMI. *Atmospheric Chemistry and Physics*, **18 (15)**, 11 277–11 287, https://doi.org/10.5194/acp-18-11277-2018.

Ayarzagüena, B., and Coauthors, 2020: Uncertainty in the Response of Sudden Stratospheric Warmings and Stratosphere-Troposphere Coupling to Quadrupled CO2 Concentrations in CMIP6 Models. *Journal of Geophysical Research: Atmospheres*, **125 (6)**, e2019JD032 345, https://doi.org/10.1029/2019JD032345.

Baldwin, M. P., 2001: Annular modes in global daily surface pressure. *Geophysical Research Letters*, **28 (21)**, 4115–4118, https://doi.org/10.1029/2001GL013564.

Baldwin, M. P., and T. J. Dunkerton, 1999: Propagation of the Arctic Oscillation from the stratosphere to the troposphere. *Journal of Geophysical Research: Atmospheres*, **104 (D24)**, 30 937–30 946, https://doi.org/https://doi.org/10.1029/1999JD900445.

Baldwin, M. P., and T. J. Dunkerton, 2001: Stratospheric harbingers of anomalous weather regimes. *Science*, **294 (5542)**, 581–4.

Baldwin, M. P., and Coauthors, 2021: Sudden Stratospheric Warmings. *Reviews of Geophysics*, **59 (1)**, e2020RG000 708, https://doi.org/10.1029/2020RG000708.

Bell, C. J., L. J. Gray, and J. Kettleborough, 2010: Changes in Northern Hemisphere stratospheric variability under increased CO_2 concentrations. *Quarterly Journal of the Royal Meteorological Society*, **136 (650)**, 1181–1190, https://doi.org/10.1002/qj.633.

Birner, T., and J. R. Albers, 2017: Sudden Stratospheric Warmings and Anomalous Upward Wave Activity Flux. *Sola*, **13A (Special_Edition)**, 8–12, https://doi.org/10.2151/sola.13A-002.

Black, R. X., 2002: Stratospheric Forcing of Surface Climate in the Arctic Oscillation. *Journal of Climate*, **15 (3)**, 268–277, https://doi.org/10.1175/1520-0442(2002)015<0268:SFOSCI>2.0.CO;2.

Bretherton, C. S., C. Smith, and J. M. Wallace, 1992: An Intercomparison of Methods for Finding Coupled Patterns in Climate Data. *Journal of Climate*, **5 (6)**, 541–560, https://doi.org/10.1175/1520-0442(1992)005<0541:AIOMFF>2.0.CO;2.

Butchart, N., J. Austin, J. R. Knight, A. A. Scaife, and M. L. Gallani, 2000: The response of the stratospheric climate to projected changes in the concentrations of well-mixed greenhouse gases from 1992 to 2051. *Journal of Climate*, **13 (13)**, 2142–2159, https://doi.org/10.1175/1520-0442(2000)013<2142:TROTSC>2.0.CO;2.

Butler, A. H., D. J. Seidel, S. C. Hardiman, N. Butchart, T. Birner, and A. Match, 2015: Defining Sudden Stratospheric Warmings. *Bulletin of the American Meteorological Society*, **96 (11)**, 1913–1928, https://doi.org/10.1175/BAMS-D-13-00173.1.

Charlton, A. J., and L. M. Polvani, 2007: A New Look at Stratospheric Sudden Warmings. Part I: Climatology and Modeling Benchmarks. *Journal of Climate*, **20 (3)**, 449–469, https://doi.org/10.1175/JCLI3996.1.

Charlton-Perez, A. J., L. M. Polvani, J. Austin, and F. Li, 2008: The frequency and dynamics of stratospheric sudden warmings in the 21st century. *Journal of Geophysical Research*, **113 (D16)**, D16 116, https://doi.org/10.1029/2007JD009571.

Charney, J. G., and P. G. Drazin, 1961: Propagation of planetary-scale disturbances from the lower into the upper atmosphere. *Journal of Geophysical Research (1896-1977)*, **66 (1)**, 83–109, https://doi.org/10.1029/JZ066i001p00083.

Christiansen, B., 2000: A model study of the dynamical connection between the Arctic Oscillation and stratospheric vacillations. *Journal of Geophysical Research: Atmospheres*, **105 (D24)**, 29 461–29 474, https://doi.org/10.1029/2000JD900542.

Christiansen, B., 2001: Downward propagation of zonal mean zonal wind anomalies from the stratosphere to the troposphere: Model and reanalysis. *Journal of Geophysical Research: Atmospheres*, **106 (D21)**, 27 307–27 322, https://doi.org/10.1029/2000JD000214.

Cohen, J., L. Agel, M. Barlow, C. I. Garfinkel, and I. White, 2021: Linking Arctic variability and change with extreme winter weather in the United States. *Science*, **373 (6559)**, 1116–1121, https://doi.org/10.1126/science.abi9167.

Cohen, J., and J. Jones, 2011: Tropospheric Precursors and Stratospheric Warmings. *Journal of Climate*, **24 (24)**, 6562–6572, https://doi.org/10.1175/2011JCLI4160.1.

Domeisen, D. I. V., L. Sun, and G. Chen, 2013: The role of synoptic eddies in the tropospheric response to stratospheric variability. *Geophysical Research Letters*, **40 (18)**, 4933–4937, https://doi.org/10.1002/grl.50943.

Domeisen, D. I. V., and Coauthors, 2020: The Role of the Stratosphere in Subseasonal to Seasonal Prediction: 2. Predictability Arising From Stratosphere-Troposphere Coupling. *Journal of Geophysical Research: Atmospheres*, **125 (2)**, e2019JD030 923, https://doi.org/10.1029/2019JD030923.

Dunn-Sigouin, E., and T. A. Shaw, 2015: Comparing and contrasting extreme stratospheric events, including their coupling to the tropospheric circulation. *Journal of Geophysical Research: Atmospheres*, **120 (4)**, 1374–1390, https://doi.org/10.1002/2014JD022116.

Edmon, H. J., B. J. Hoskins, and M. E. McIntyre, 1980: Eliassen-Palm Cross Sections for the Troposphere. *Journal of the Atmospheric Sciences*, **37 (12)**, 2600–2616, https://doi.org/10.1175/1520-0469(1980)037<2600:EPCSFT>2.0.CO;2.

Esler, J. G., and R. K. Scott, 2005: Excitation of Transient Rossby Waves on the Stratospheric Polar Vortex and the Barotropic Sudden Warming. *Journal of the Atmospheric Sciences*, **62 (10)**, 3661–3682, https://doi.org/10.1175/JAS3557.1.

Garfinkel, C. I., D. L. Hartmann, and F. Sassi, 2010: Tropospheric Precursors of Anomalous Northern Hemisphere Stratospheric Polar Vortices. *Journal of Climate*, **23 (12)**, 3282–3299, https://doi.org/10.1175/2010JCLI3010.1.

Hamouda, M. E., C. Pasquero, and E. Tziperman, 2021: Decoupling of the Arctic Oscillation and North Atlantic Oscillation in a warmer climate. *Nature Climate Change*, **11 (2)**, 137–142, https://doi.org/10.1038/s41558-020-00966-8.

Harnik, N., 2002: The Evolution of a Stratospheric Wave Packet. *Journal of the Atmospheric Sciences*, **59 (2)**, 202–217, https://doi.org/10.1175/1520-0469(2002)059<0202:TEOASW>2.0.CO;2.

Harnik, N., 2009: Observed stratospheric downward reflection and its relation to upward pulses of wave activity. *Journal of Geophysical Research: Atmospheres*, **114 (D8)**, https://doi.org/10.1029/2008JD010493.

Harnik, N., and R. S. Lindzen, 2001: The Effect of Reflecting Surfaces on the Vertical Structure and Variability of Stratospheric Planetary Waves. *Journal of the Atmospheric Sciences*, **58 (19)**, 2872–2894, https://doi.org/10.1175/1520-0469(2001)058<2872:TEORSO>2.0.CO;2.

Hartley, D. E., J. T. Villarin, R. X. Black, and C. A. Davis, 1998: A new perspective on the dynamical link between the stratosphere and troposphere. *Nature*, **391 (6666)**, 471–474.

Hirota, I., and Y. Sato, 1969: Periodic variation of the winter stratospheric circulation and intermittent vertical propagation. *Journal of the Meteorological Society of Japan. Ser. II*, **47 (5)**, 390–402, https://doi.org/10.2151/jmsj1965.47.5_390.

Hitchcock, P., and I. R. Simpson, 2014: The Downward Influence of Stratospheric Sudden Warmings. *Journal of the Atmospheric Sciences*, **71 (10)**, 3856–3876, https://doi.org/10.1175/JAS-D-14-0012.1.

Hitchcock, P., and I. R. Simpson, 2016: Quantifying Eddy Feedbacks and Forcings in the Tropospheric Response to Stratospheric Sudden Warmings. *Journal of the Atmospheric Sciences*, **73 (9)**, 3641–3657, https://doi.org/10.1175/JAS-D-16-0056.1.

Holton, J. R., and C. Mass, 1976: Stratospheric Vacillation Cycles. *Journal of the Atmospheric Sciences*, **33 (11)**, 2218–2225, https://doi.org/10.1175/1520-0469(1976)033<2218:SVC>2.0.CO;2.

Hurrell, J. W., Y. Kushnir, G. Ottersen, and M. Visbeck, 2003: An overview of the North Atlantic Oscillation. *Geophysical Monograph Series*, J. W. Hurrell, Y. Kushnir, G. Ottersen, and M. Visbeck, Eds., Vol. 134, American Geophysical Union, Washington, D. C., 1–35, https://doi.org/10.1029/134GM01.

Jucker, M., and T. Reichler, 2018: Dynamical Precursors for Statistical Prediction of Stratospheric Sudden Warming Events. *Geophysical Research Letters*, **45 (23)**, 13,124–13,132, https://doi.org/10.1029/2018GL080691.

Kang, W., and E. Tziperman, 2017: More Frequent Sudden Stratospheric Warming Events due to Enhanced MJO Forcing Expected in a Warmer Climate. *Journal of Climate*, **30 (21)**, 8727–8743, https://doi.org/10.1175/JCLI-D-17-0044.1.

Karoly, D. J., and B. J. Hoskins, 1982: Three dimensional propagation of planetary waves. *Journal of the Meteorological Society of Japan. Ser. II*, **60 (1)**, 109–123.

Kidston, J., A. A. Scaife, S. C. Hardiman, D. M. Mitchell, N. Butchart, M. P. Baldwin, and L. J. Gray, 2015: Stratospheric influence on tropospheric jet streams, storm tracks and surface weather. *Nature Geoscience*, **8 (6)**, 433–440, https://doi.org/10.1038/ngeo2424.

Kim, J., S.-W. Son, E. P. Gerber, and H.-S. Park, 2017: Defining Sudden Stratospheric Warming in Climate Models: Accounting for Biases in Model Climatologies. *Journal of Climate*, **30 (14)**, 5529–5546, https://doi.org/10.1175/JCLI-D-16-0465.1.

Kodera, K., Y. Kuroda, and S. Pawson, 2000: Stratospheric sudden warmings and slowly propagating zonal-mean zonal wind anomalies. *Journal of Geophysical Research: Atmospheres*, **105 (D10)**, 12 351–12 359, https://doi.org/10.1029/2000JD900095.

Kodera, K., H. Mukougawa, P. Maury, M. Ueda, and C. Claud, 2016: Absorbing and reflecting sudden stratospheric warming events and their relationship with tropospheric circulation. *Journal of Geophysical Research: Atmospheres*, **121 (1)**, 80–94, https://doi.org/10.1002/2015JD023359.

Kolstad, E. W., T. Breiteig, and A. A. Scaife, 2010: The association between stratospheric weak polar vortex events and cold air outbreaks in the Northern Hemisphere. *Quarterly Journal of the Royal Meteorological Society*, **136 (649)**, 886–893, https://doi.org/10.1002/qj.620.

Kretschmer, M., J. Cohen, V. Matthias, J. Runge, and D. Coumou, 2018a: The different stratospheric influence on cold-extremes in Eurasia and North America. *npj Climate and Atmospheric Science*, **1 (1)**, 1–10, https://doi.org/10.1038/s41612-018-0054-4.

Kretschmer, M., D. Coumou, L. Agel, M. Barlow, E. Tziperman, and J. Cohen, 2018b: More-Persistent Weak Stratospheric Polar Vortex States Linked to Cold Extremes. *Bulletin of the American Meteorological Society*, **99 (1)**, 49–60, https://doi.org/10.1175/BAMS-D-16-0259.1.

Kuroda, Y., and K. Kodera, 1999: Role of planetary waves in the stratosphere-troposphere coupled variability in the northern hemisphere winter. *Geophysical Research Letters*, **26 (15)**, 2375–2378, https://doi.org/10.1029/1999GL900507.

Labitzke, K., and M. Kunze, 2009: On the remarkable Arctic winter in 2008/2009. *Journal of Geophysical Research: Atmospheres*, **114 (D1)**, https://doi.org/10.1029/2009JD012273.

Lee, S. H., J. C. Furtado, and A. J. Charlton-Perez, 2019: Wintertime North American Weather Regimes and the Arctic Stratospheric Polar Vortex. *Geophysical Research Letters*, **46 (24)**, 14 892–14 900, https://doi.org/10.1029/2019GL085592.

Lehtonen, I., and A. Y. Karpechko, 2016: Observed and modeled tropospheric cold anomalies associated with sudden stratospheric warmings. *Journal of Geophysical Research: Atmospheres*, **121 (4)**, 1591–1610, https://doi.org/10.1002/2015JD023860.

Limpasuvan, V., D. W. J. Thompson, and D. L. Hartmann, 2004: The Life Cycle of the Northern Hemisphere Sudden Stratospheric Warmings. *Journal of Climate*, **17 (13)**, 2584–2596, https://doi.org/10.1175/1520-0442(2004)017<2584:TLCOTN>2.0.CO;2.

Lubis, S. W., K. Matthes, N.-E. Omrani, N. Harnik, and S. Wahl, 2016: Influence of the Quasi-Biennial Oscillation and Sea Surface Temperature Variability on Downward Wave Coupling in the Northern Hemisphere. *Journal of the Atmospheric Sciences*, **73 (5)**, 1943–1965, https://doi.org/10.1175/JAS-D-15-0072.1.

Marshall, J., and Coauthors, 2001: North Atlantic climate variability: phenomena, impacts and mechanisms. *International Journal of Climatology*, **21 (15)**, 1863–1898, https://doi.org/10.1002/joc.693.

Martius, O., L. M. Polvani, and H. C. Davies, 2009: Blocking precursors to stratospheric sudden warming events. *Geophysical Research Letters*, **36 (14)**, https://doi.org/10.1029/2009GL038776.

Matsuno, T., 1971: A Dynamical Model of the Stratospheric Sudden Warming. *Journal of the Atmospheric Sciences*, **28 (8)**, 1479–1494, https://doi.org/10.1175/1520-0469(1971)028<1479:ADMOTS>2.0.CO;2.

McIntyre, M. E., and T. N. Palmer, 1984: The 'surf zone' in the stratosphere. *Journal of Atmospheric and Terrestrial Physics*, **46 (9)**, 825–849, https://doi.org/10.1016/0021-9169(84)90063-1.

McLandress, C., and T. G. Shepherd, 2009: Impact of climate change on stratospheric sudden warmings as simulated by the Canadian middle atmosphere model. *Journal of Climate*, **22 (20)**, 5449–5463, https://doi.org/10.1175/2009JCLI3069.1.

Mitchell, D. M., L. J. Gray, J. Anstey, M. P. Baldwin, and A. J. Charlton-Perez, 2013: The Influence of Stratospheric Vortex Displacements and Splits on Surface Climate. *Journal of Climate*, **26 (8)**, 2668–2682, https://doi.org/10.1175/JCLI-D-12-00030.1.

Mitchell, D. M., S. M. Osprey, L. J. Gray, N. Butchart, S. C. Hardiman, A. J. Charlton-Perez, and P. Watson, 2012: The effect of climate change on the variability of the northern hemisphere stratospheric polar vortex. *Journal of the Atmospheric Sciences*, **69 (8)**, 2608–2618, https://doi.org/10.1175/JAS-D-12-021.1.

911 North, G. R., T. L. Bell, R. F. Cahalan, and F. J. Moeng, 1982: Sampling Errors in the Estimation
912 of Empirical Orthogonal Functions. *Monthly Weather Review*, **110 (7)**, 699–706, https://doi.org/
913 10.1175/1520-0493(1982)110<0699:SEITEO>2.0.CO;2.

914 Palmer, T. N., 1981: Aspects of stratospheric sudden warmings studied from a transformed
915 Eulerian-mean viewpoint. *Journal of Geophysical Research: Oceans*, **86 (C10)**, 9679–9687,
916 https://doi.org/10.1029/JC086iC10p09679.

917 Perlwitz, J., and H.-F. Graf, 1995: The Statistical Connection between Tropospheric and Strato-
918 spheric Circulation of the Northern Hemisphere in Winter. *Journal of Climate*, **8 (10)**, 2281–
919 2295, https://doi.org/10.1175/1520-0442(1995)008<2281:TSCBTA>2.0.CO;2.

920 Perlwitz, J., and N. Harnik, 2003: Observational Evidence of a Stratospheric Influence on the Tro-
921 posphere by Planetary Wave Reflection. *Journal of Climate*, **16 (18)**, 3011–3026, https://doi.org/
922 10.1175/1520-0442(2003)016<3011:OEOASI>2.0.CO;2.

923 Perlwitz, J., and N. Harnik, 2004: Downward Coupling between the Stratosphere and Troposphere:
924 The Relative Roles of Wave and Zonal Mean Processes. *Journal of Climate*, **17 (24)**, 4902–4909,
925 https://doi.org/10.1175/JCLI-3247.1.

926 Plumb, R. A., 2010: Planetary Waves and the Extratropical Winter Stratosphere. *The Stratosphere:*
927 *Dynamics, Transport, and Chemistry*, **190**, 23–41.

928 Plumb, R. A., and K. Semeniuk, 2003: Downward migration of extratropical zonal wind
929 anomalies. *Journal of Geophysical Research: Atmospheres*, **108 (D7)**, https://doi.org/10.1029/
930 2002JD002773.

931 Polvani, L. M., and D. W. Waugh, 2004: Upward Wave Activity Flux as a Precursor to Extreme
932 Stratospheric Events and Subsequent Anomalous Surface Weather Regimes. *Journal of Climate*,
933 **17 (18)**, 3548–3554, https://doi.org/10.1175/1520-0442(2004)017<3548:UWAFAA>2.0.CO;2.

934 Quiroz, R. S., 1986: The association of stratospheric warmings with tropospheric blocking.
935 *Journal of Geophysical Research: Atmospheres*, **91 (D4)**, 5277–5285, https://doi.org/10.1029/
936 JD091iD04p05277.

937 Randel, W. J., 1987: A Study of Planetary Waves in the Southern Winter Troposphere and
938 Stratosphere. Part I: Wave Structure and Vertical Propagation. *Journal of the Atmospheric*

Sciences, **44 (6)**, 917–935, https://doi.org/10.1175/1520-0469(1987)044<0917:ASOPWI>2.0.CO;2.

Rao, J., and C. I. Garfinkel, 2021: CMIP5/6 models project little change in the statistical characteristics of sudden stratospheric warmings in the 21st century. *Environmental Research Letters*, **16 (3)**, 034 024, https://doi.org/10.1088/1748-9326/abd4fe.

Savitzky, A., and M. J. E. Golay, 1964: Smoothing and Differentiation of Data by Simplified Least Squares Procedures. *Analytical Chemistry*, **36 (8)**, 1627–1639, https://doi.org/10.1021/ac60214a047.

Scaife, A. A., J. R. Knight, G. K. Vallis, and C. K. Folland, 2005: A stratospheric influence on the winter NAO and North Atlantic surface climate. *Geophysical Research Letters*, **32 (18)**, https://doi.org/10.1029/2005GL023226.

Schimanke, S., T. Spangehl, H. Huebener, and U. Cubasch, 2013: Variability and trends of major stratospheric warmings in simulations under constant and increasing GHG concentrations. *Climate Dynamics*, **40 (7-8)**, 1733–1747, https://doi.org/10.1007/s00382-012-1530-x.

Shaw, T. A., J. Perlwitz, and N. Harnik, 2010: Downward Wave Coupling between the Stratosphere and Troposphere: The Importance of Meridional Wave Guiding and Comparison with Zonal-Mean Coupling. *Journal of Climate*, **23 (23)**, 6365–6381, https://doi.org/10.1175/2010JCLI3804.1.

Sigmond, M., J. F. Scinocca, V. V. Kharin, and T. G. Shepherd, 2013: Enhanced seasonal forecast skill following stratospheric sudden warmings. *Nature Geoscience*, **6 (2)**, 98–102, https://doi.org/10.1038/ngeo1698.

Simpson, I. R., M. Blackburn, and J. D. Haigh, 2009: The Role of Eddies in Driving the Tropospheric Response to Stratospheric Heating Perturbations. *Journal of the Atmospheric Sciences*, **66 (5)**, 1347–1365, https://doi.org/10.1175/2008JAS2758.1.

Smith, K. L., and P. J. Kushner, 2012: Linear interference and the initiation of extratropical stratosphere-troposphere interactions. *Journal of Geophysical Research: Atmospheres*, **117 (D13)**, https://doi.org/10.1029/2012JD017587.

966 Thompson, D. W. J., M. P. Baldwin, and S. Solomon, 2005: Stratosphere–Troposphere Coupling in
967 the Southern Hemisphere. *Journal of the Atmospheric Sciences*, **62 (3)**, 708–715, https://doi.org/
968 10.1175/JAS-3321.1.

969 Thompson, D. W. J., M. P. Baldwin, and J. M. Wallace, 2002: Stratospheric Connection to
970 Northern Hemisphere Wintertime Weather: Implications for Prediction. *Journal of Climate*,
971 **15 (12)**, 1421–1428, https://doi.org/10.1175/1520-0442(2002)015<1421:SCTNHW>2.0.CO;2.

972 Thompson, D. W. J., S. Lee, and M. P. Baldwin, 2003: Atmospheric Processes Governing the
973 Northern Hemisphere Annular Mode/North Atlantic Oscillation. *The North Atlantic Oscillation:*
974 *Climatic Significance and Environmental Impact*, American Geophysical Union (AGU), 81–112,
975 https://doi.org/10.1029/134GM05.

976 Thompson, D. W. J., and J. M. Wallace, 2001: Regional climate impacts of the Northern Hemi-
977 sphere annular mode. *Science*, **293 (5527)**, 85–9.

978 Tomassini, L., E. P. Gerber, M. P. Baldwin, F. Bunzel, and M. Giorgetta, 2012: The role of
979 stratosphere-troposphere coupling in the occurrence of extreme winter cold spells over northern
980 Europe. *Journal of Advances in Modeling Earth Systems*, **4 (4)**, https://doi.org/https://doi.org/
981 10.1029/2012MS000177.

982 Wallace, J. M., 2000: North Atlantic Oscillation/annular mode: Two paradigms—one phe-
983 nomenon. *Quarterly Journal of the Royal Meteorological Society*, **126 (564)**, 791–805,
984 https://doi.org/10.1002/qj.49712656402.

985 White, I. P., C. I. Garfinkel, E. P. Gerber, M. Jucker, P. Hitchcock, and J. Rao, 2020: The Generic
986 Nature of the Tropospheric Response to Sudden Stratospheric Warmings. *Journal of Climate*,
987 **33 (13)**, 5589–5610, https://doi.org/10.1175/JCLI-D-19-0697.1.

988 Wittman, M. A. H., L. M. Polvani, R. K. Scott, and A. J. Charlton, 2004: Stratospheric influence on
989 baroclinic lifecycles and its connection to the Arctic Oscillation. *Geophysical Research Letters*,
990 **31 (16)**, https://doi.org/10.1029/2004GL020503.

991 Yu, Y., M. Cai, C. Shi, and R. Ren, 2018: On the Linkage among Strong Stratospheric Mass
992 Circulation, Stratospheric Sudden Warming, and Cold Weather Events. *Monthly Weather Review*,
993 **146 (9)**, 2717–2739, https://doi.org/10.1175/MWR-D-18-0110.1.

Zhang, P., Y. Wu, G. Chen, and Y. Yu, 2020: North American cold events following sudden stratospheric warming in the presence of low Barents-Kara Sea sea ice. *Environmental Research Letters*, **15 (12)**, 124 017, https://doi.org/10.1088/1748-9326/abc215.

Zhang, Y., D. Si, Y. Ding, D. Jiang, Q. Li, and G. Wang, 2022: Influence of Major Stratospheric Sudden Warming on the Unprecedented Cold Wave in East Asia in January 2021. *Advances in Atmospheric Sciences*, **39 (4)**, 576–590, https://doi.org/10.1007/s00376-022-1318-9.